Electronic Supplementary Material (ESI) for Inorganic Chemistry Frontiers.


# *Electronic Supplementary Information*

## Combination of dimensional reduction and active site addition strategies for preparing unique {$RE_9$}-cluster-based MOFs: efficient $CO_2$ fixation and Knoevenagel condensation

Ying Zhao,‡[a] Dan Wu,‡[b,c] Yidan Qiao,[a] Guo-Ping Yang,*[b] Lu-Fang Ma*[a,b] and Yao-Yu Wang[b]

[a] *College of Chemistry and Chemical Engineering, Henan Key Laboratory of Function-Oriented Porous Materials, Luoyang Normal University, Luoyang 471934, P.R. China.*

[b] *College of Chemistry and Materials Science, Northwest University, Xi'an 710127, P.R. China.*

[c] *Shaanxi Applied Physics and Chemistry Research Institute, Xi'an 710061, P.R. China.*

*E-mail: ygp@nwu.edu.cn; mazhuxp@126.com.*

‡*These authors contributed equally to this work.*

**Experimental section**

**Materials and general methods.** All the reagents and solvents were purchased to use without further purification in the experiments. And the $H_2$pddb ligand was bought from Jinan Camolai Trading Company. Fourier transform infrared (FT-IR) spectra were examined on Bruker EQUINOX-55 spectrophotometer in 4000 ~ 400 $cm^{-1}$ (KBr pellets). Powder X-ray diffraction (PXRD) patterns were investigated through Bruker D8 ADVANCE X-ray powder diffractometer with Cu K*a* radiation ($\lambda$ = 1.5418 Å). Thermogravimetric analyses (TGA) were tested on NETZSCH STA 449C microanalyzer ($N_2$ atmosphere, 10 ℃ $min^{-1}$). Inductively coupled plasma mass spectrometry (ICP-MS) was performed on an Agilent 7900 instrument. The gas sorption isotherms were tested on ASAP 2020 M sorption equipment. $^1$H NMR spectra were recorded at 298 K on Bruker AVANCE III 400/600 spectrometers.

**Synthesis of $\{[Me_2NH_2]_4[RE_9(pddb)_6(\mu_3\text{-}O)_2(\mu_3\text{-}OH)_{12}(H_2O)_{1.5}(HCO_2)_3]\cdot 6.5DMF\cdot 11H_2O\}_n$ (MOF-RE, RE = Tb, Y and Dy).** A mixture of $Tb(NO_3)_3\ 6H_2O$ (0.05 mmol, 22.7 mg) or $Y(NO_3)_3\ 6H_2O$ (0.05 mmol, 19.2 mg) or $Dy(NO_3)_3\ 6H_2O$ (0.05 mmol, 22.8 mg), $H_2$pddb (0.05 mmol, 16.0 mg), 2-fluorobenzoic acid (84.7 mg, 0.6 mmol), DMF (6 mL), $H_2O$ (0.5 mL) and $HNO_3$ (0.35 mL, 2.8 M in DMF) were placed in a Teflon-lined stainless steel vessel, heated to 120 ℃ for 72 h and then cooled to room temperature at a rate of 10 ℃ $h^{-1}$ to form colorless hexagonal crystals. Yield: 82% for **MOF-Tb**; 88% for **MOF-Y**; 85% for **MOF-Dy**. FT-IR ($cm^{-1}$, Figure S4) for **MOF-Tb**: 3488 (m), 1658 (s), 1609 (s), 1575 (s), 1404 (s), 1173 (w), 1102 (m), 1014 (m), 879 (m), 778 (s), 720 (m), 660 (w), 572 (w), 525 (w), 483 (m). FT-IR ($cm^{-1}$, KBr pellets) for **MOF-Y**: 3428 (m), 1658 (s), 1604 (s), 1577 (s), 1417 (s), 1297 (w), 1257 (w), 1164 (w), 1097 (m), 1017 (w), 871 (w), 777 (s), 697 (w), 657 (w), 564 (w), 484 (m), 417 (w). FT-IR ($cm^{-1}$, KBr pellets) for **MOF-Dy**: 3427 (m), 1653 (s), 1613 (s), 1587 (s), 1413 (s), 1304 (w), 1250 (w), 1170 (w), 1103 (m), 1010 (m), 877 (m), 770 (s), 703 (w), 663 (w), 570 (w), 490 (m).

**Crystallographic data collection and refinement.** The single-crystal diffraction data were recorded on a Bruker SMART APEX II CCD detector by Mo-Kα radiation (λ = 0.71073 Å) for **MOF-RE**. The structures of MOFs were solved via the direct methods and refined through the full-matrix least-squares method based on $F^2$ on the SHELXL and Olex2 program.[1] All non-hydrogen atoms were refined anisotropically with the hydrogen atoms being calculated and

assigned their ideal positions with isotropic displacement factors. The final formulae of **MOF-RE** were determined by combination of the single-crystal structure, elemental analysis and TGA together. The pertinent crystal data are listed in Table 1. These CCDC numbers are 2216930-2216932 for **MOF-RE (RE = Tb, Y, Dy)**, respectively.

**Thermogravimetric study.** The thermal stability and structural composition of **MOF-Tb**, **MOF-Y** and **MOF-Dy** were determined by TGA. The thermal stability of **MOF-Tb** was analyzed as an example. As shown in Figure S5, with the increase of temperature, the weightlessness of **MOF-Tb** went through three processes in turn. The initial 5.01% weight loss before 100 ℃ was assigned to the removal of lattice water molecules, similar to the theoretical content of 5.05%. During 100-230 ℃, a sharp weight loss of 18.1% occurred, which should be attributed to the removal of DMF solvent and coordinated aqueous ligands with the theoretical value of 17.8%. Finally, the framework of **MOF-Tb** completely collapsed when the temperature exceeded 420 ℃.

**Gas sorption measurements.** Prior to the adsorption determination, the freshly prepared sample (60 mg) was activated by vacuum at 200 ℃ for 4 h until a pressure of 5 $\mu$mHg to obtain the activated **MOF-Tba**. Gas adsorption measurements were carried out using ASAP 2020 M sorption equipment. As the center-controlled air condition was set up at 25 ℃, a water bath of 25 ℃ was used for adsorption isotherms at 298 K, whereas liquid nitrogen, dry ice-acetone baths and ice-water baths were used for the isotherms at 77 K, 195 K and 273 K, respectively. Pore size distribution (PSD) data was obtained from the 77 K $N_2$ sorption isotherms based on the nonlocal density functional theory (NLDFT) model.

**General procedure for catalytic experiment operation.** The chemical fixation of $CO_2$ was performed by coupling $CO_2$ and epoxides under mild conditions. The styrene oxide (20 mmol) as model reactant, cocatalyst *n*-$Bu_4NBr$ (5 mol%), and catalyst **MOF-Tba** (0.125 mol%, based on the {$Tb_9$} cluster) were transferred into reaction flasks and stirred at a certain temperature (from room temperature to 60 ℃). The reaction flasks were subjected to vacuum, and $CO_2$-containing balloons were placed on the reaction flasks. Finally, the products were collected and their $^1H$ NMR spectrum was recorded in Chloroform-*d* solution. As for the Knoevenagel condensation reaction, substrates of 10 mmol benzaldehydes and 20 mmol malononitrile in the presence of activated **MOF-Tba** (0.25 mol%, based on the {$Tb_9$} cluster) was conducted in a magnetically

stirred round-bottom quartz flask. After the reaction was completed, the catalytic yield of this Knoevenagel condensation reaction was verified by the $^{1}$H NMR spectroscopy in Chloroform-*d* solution. Moreover, after each catalytic cycle, the solid catalysts were collected by centrifugation, washed with DMF, and dried under vacuum.

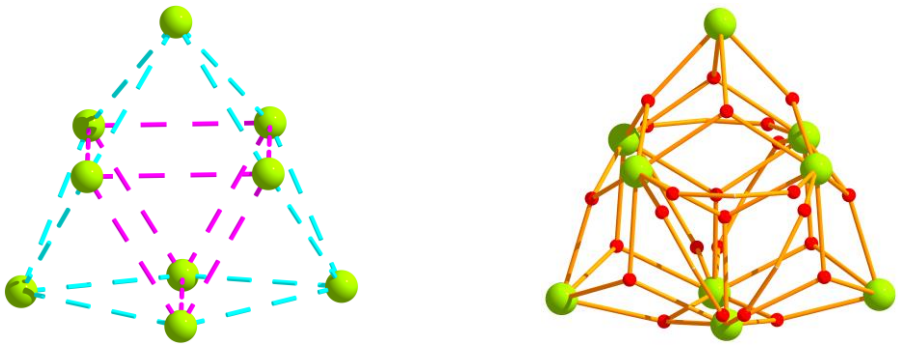

**(a)** **(b)**

**Figure S1.** (a) The nine RE ions in the $[RE_9(\mu_3\text{-}O)_2(\mu_3\text{-}OH)_{12}(O_2C\text{-})_{12}(HCO_2)_3(H_2O)_3]$ cluster form a tricapped trigonal prism arrangement; (b) Illustration of the nonanuclear core structure.

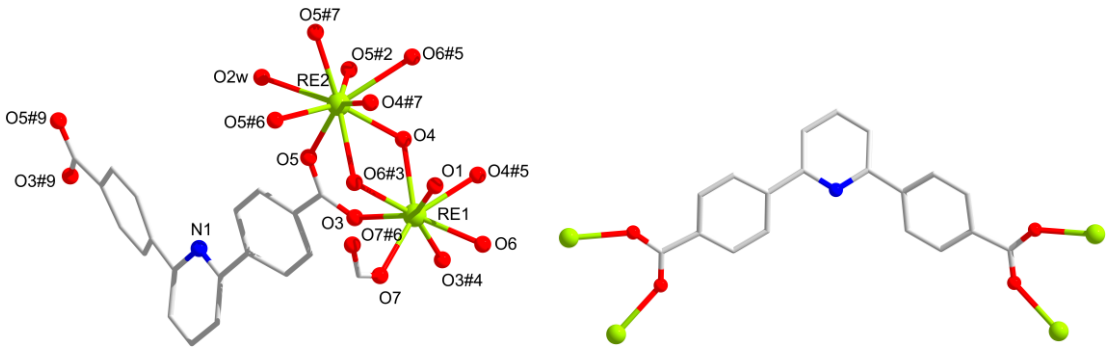


**(a)** **(b)**

**Figure S2.** (a) Coordination environments of RE(III) ions in **MOF-RE**; (b) Coordination mode of the pddb$^{2-}$ ligand in **MOF-RE**.

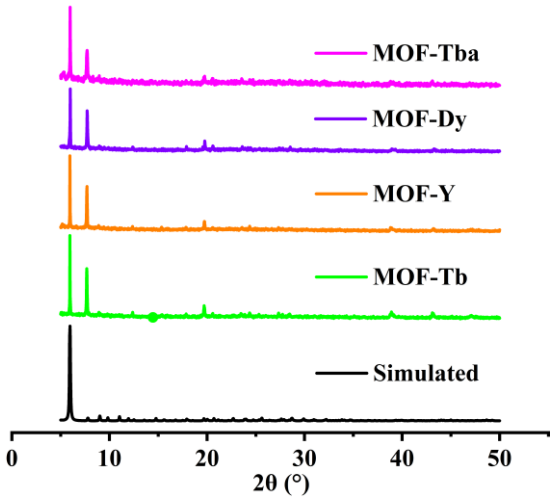


**Figure S3.** PXRD patterns of the as-synthesized and activated samples.

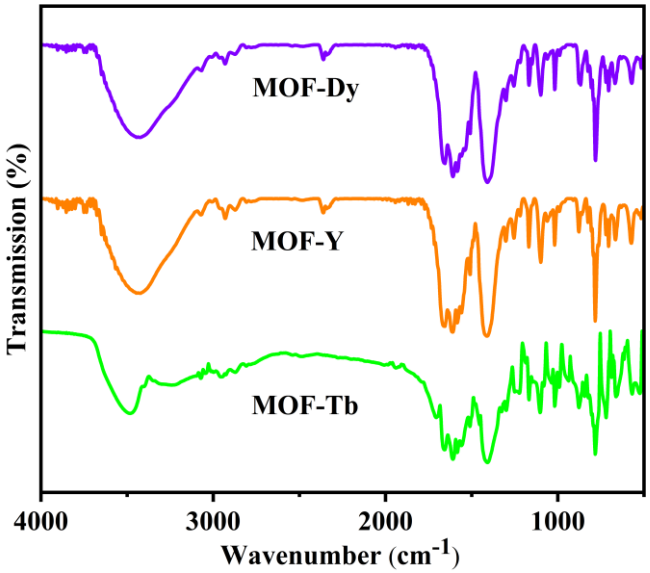


**Figure S4.** The FT-IR spectra of the as-synthesized samples.

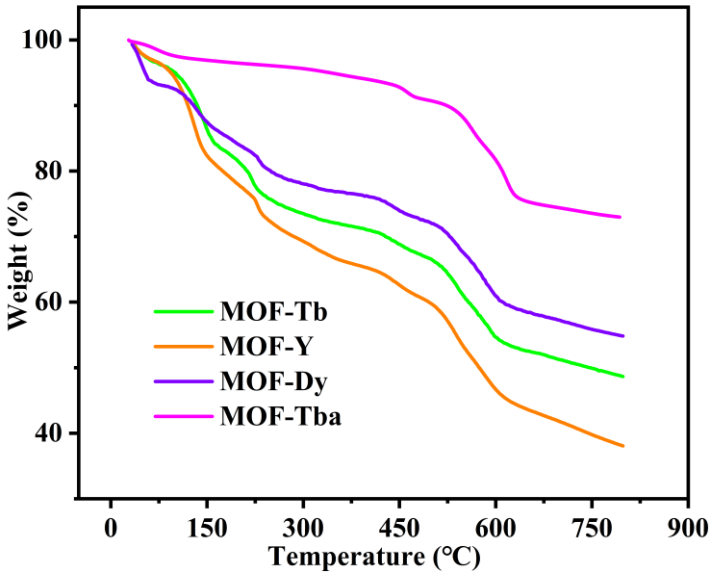


**Figure S5.** TGA curves of the as-synthesized products and activated sample.

**Adsorption enthalpy calculation** The $CO_2$, $CH_4$, $C_2H_2$, $C_2H_4$ and $C_2H_6$ adsorption enthalpy ($Q_{st}$) of **MOF-Tba** was calculated using adsorption data at 273 K and 298 K. A virial-type expression (equation S1) was used to fit these data, and then the $Q_{st}$ was then calculated by the expression given by equation S2.

$$\ln P = \ln N + 1/\mathrm{T}\sum_{i=0}^{m} a_i N^i + \sum_{i=0}^{n} b_i N^i \quad \text{(S1)}$$

$$Q_{\mathrm{st}} = -R\sum_{i=0}^{m} a_i N^i \quad \text{(S2)}$$

Here $P$ is the pressure, $N$ is the adsorbed amount, $T$ is the temperature, $a_i$ and $b_i$ are virial coefficients, and $m$ and $N$ are the number of coefficients used to describe the isotherms. $Q_{st}$ is the coverage-dependent enthalpy of adsorption and $R$ is the universal gas constant.

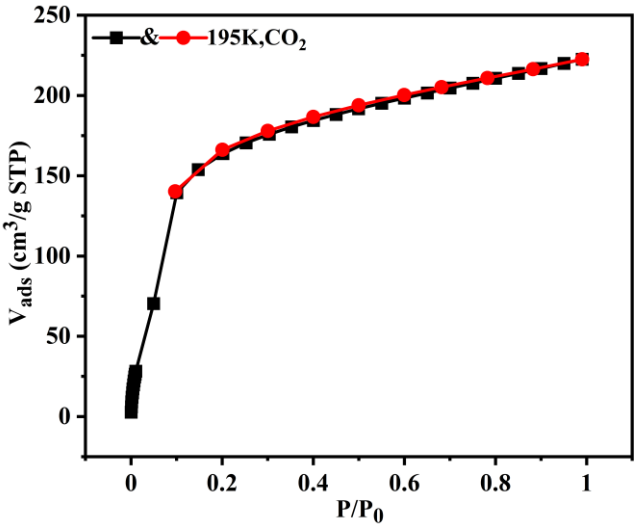


**Figure S6.** Gas adsorption isotherm for $CO_2$ at 195 K.

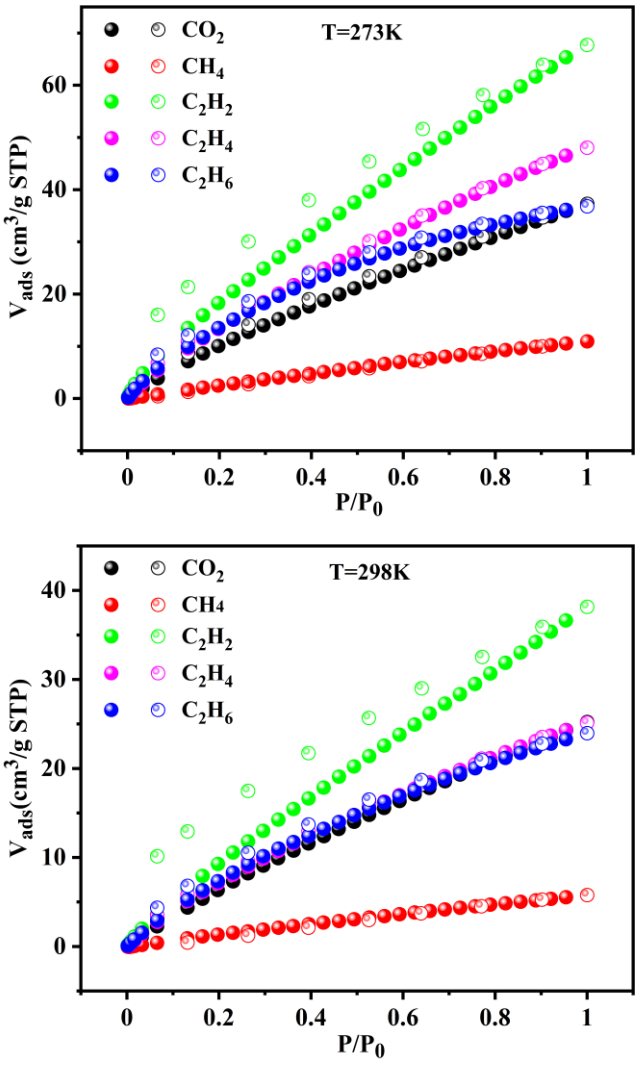


**(a)** **(b)**

**Figure S7.** $C_2H_n$, $CO_2$, and $CH_4$ gas sorption isotherms of **MOF-Tba** at 273 K (a) and 298 K (b).

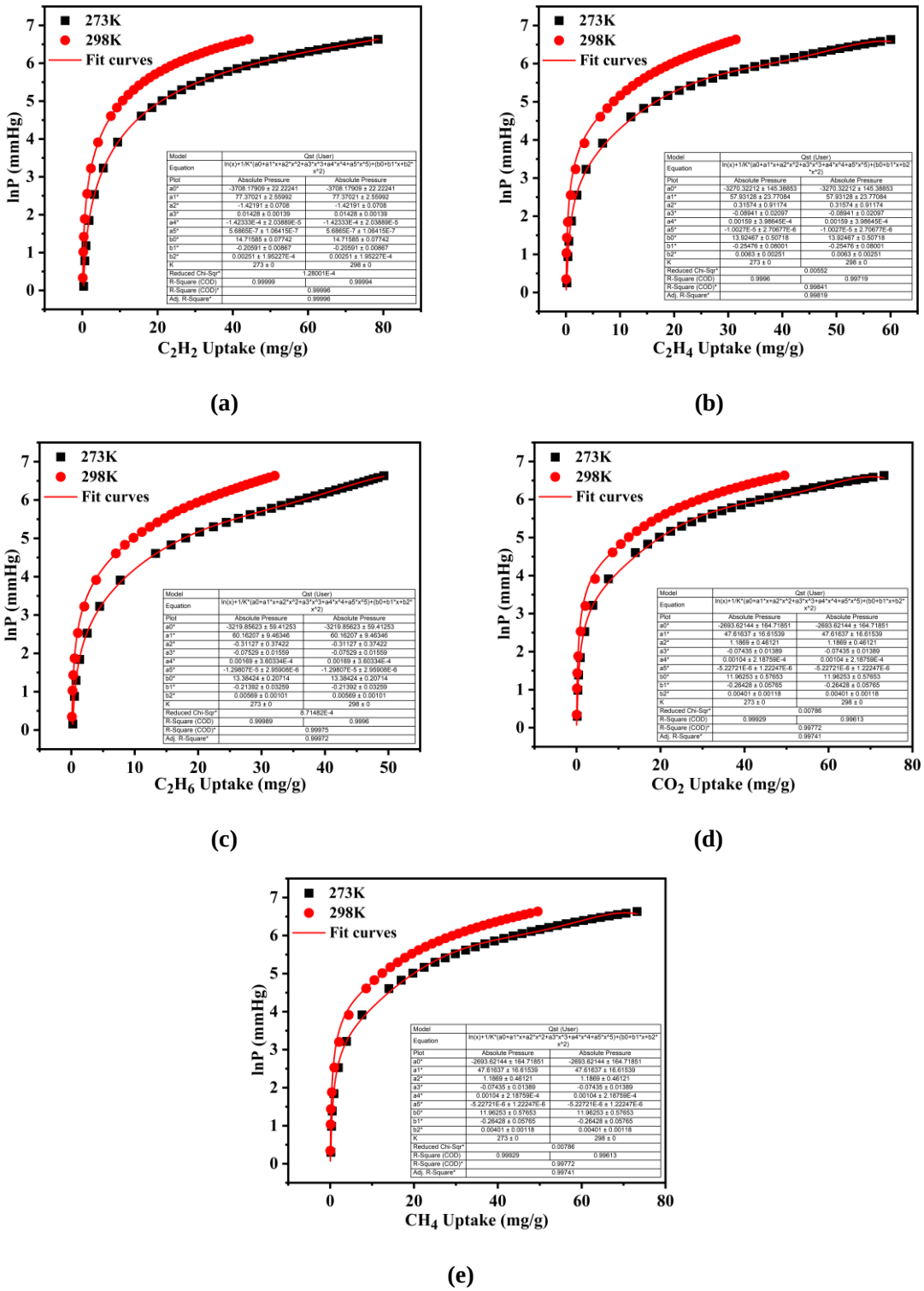


**Figure S8.** Virial fitting for sorption isotherms of $C_2H_n$ (a-c), $CO_2$ (d) and $CH_4$ (e) on **MOF-Tba**.

**Prediction of the gas adsorption selectivity by IAST:** The experimental isotherm data for pure $CO_2$, $CH_4$, $C_2H_2$, $C_2H_4$ and $C_2H_6$ (measured at 273 and 298 K) were fitted using a dual Langmuir-Freundlich (L-F) model (equation S3):

$$q = \frac{a_1 * b_1 * p^{c_1}}{1 + b_1 * p^{c_1}} + \frac{a_2 * b_2 * p^{c_2}}{1 + b_2 * p^{c_2}} \quad \text{(S3)}$$

Where $q$ and $p$ are adsorbed amounts and pressures of component $i$, respectively.

The adsorption selectivity for binary mixtures defined by equation S4

$$S_{i/j} = \frac{x_i * y_j}{x_j * y_i} \quad \text{(S4)}$$

Where $x_i$ and $x_j$ are the molar loadings in the adsorbed phase in equilibrium with the bulk gas phase with partial pressures $y_{i,}$ and $y_j$. We calculate the values of $x_i$ and $x_j$ using the Ideal Adsorbed Solution Theory (IAST) of Myers and Prausnitz.

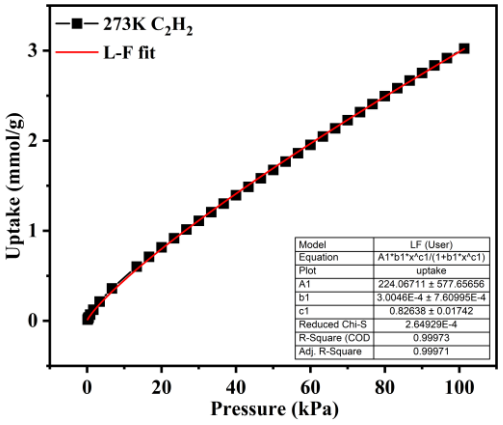


**(a)**

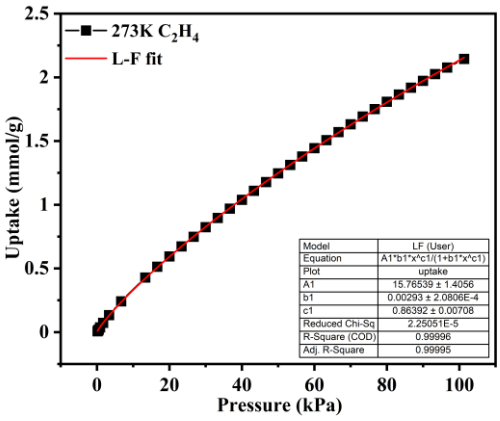


**(b)**

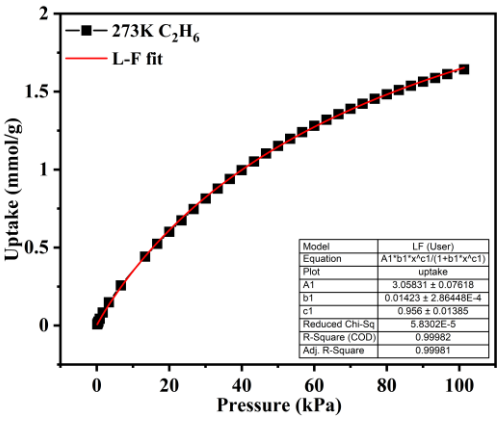


**(c)**

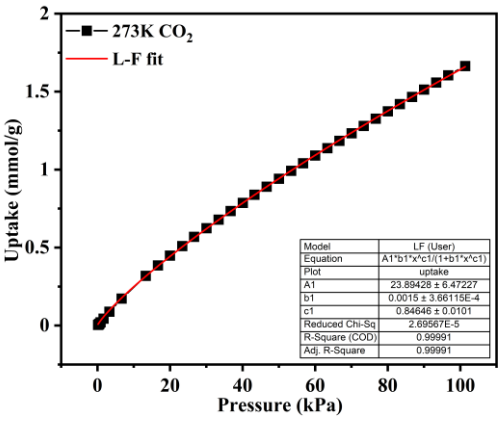


**(d)**

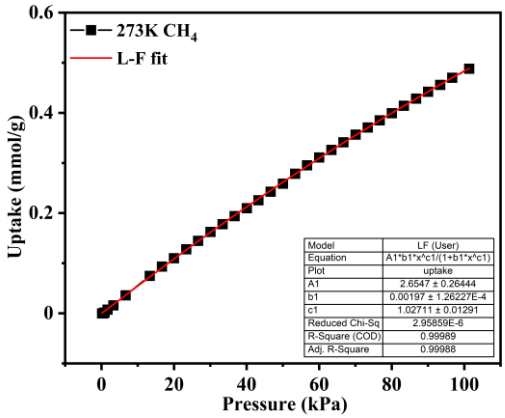


**(e)**

**Figure S9.** The graphs of the Single-site Langmuir-Freundlich equations fit for adsorption of $C_2H_n$ (a-c), $CO_2$ (d) and $CH_4$ (e) on **MOF-Tba** at 273 K.

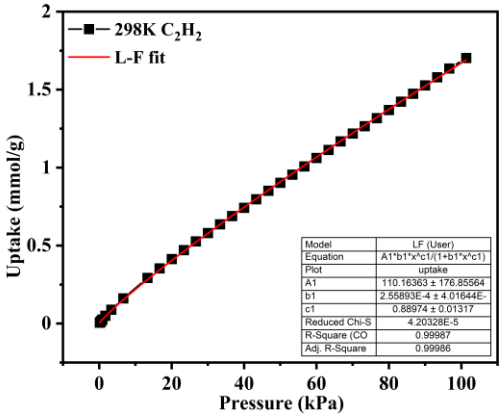


**(a)**

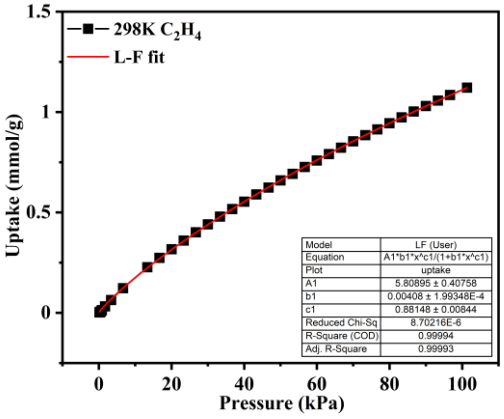


**(b)**

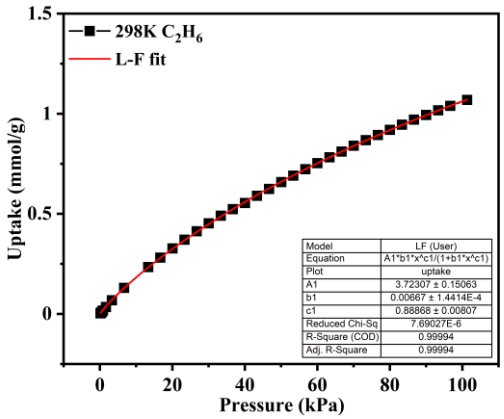


**(c)**

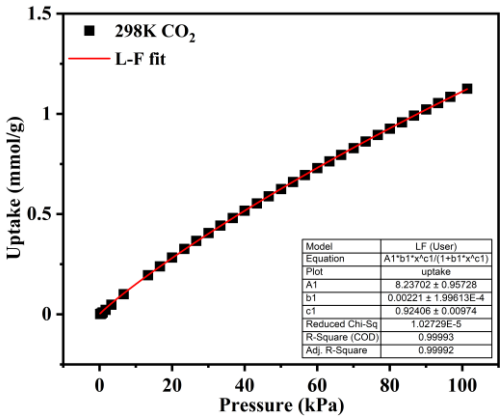


**(d)**

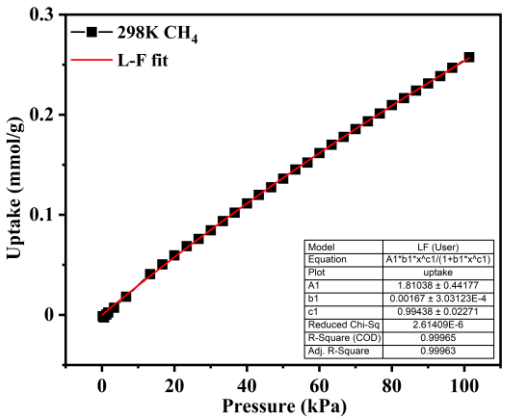


**(e)**

**Figure S10.** The graphs of the Single-site Langmuir-Freundlich equations fit for adsorption of $C_2H_n$ (a-c), $CO_2$ (d) and $CH_4$ (e) on **MOF-Tba** at 298 K.

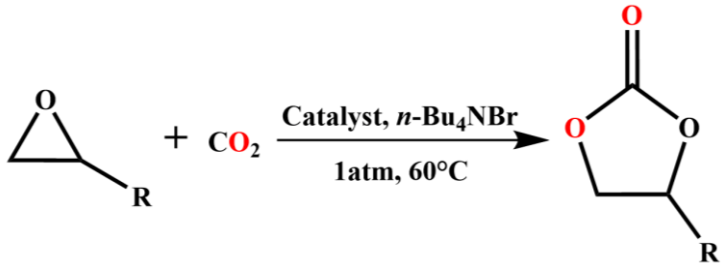


**Scheme S1.** Diagrammatic sketch of $CO_2$ fixation.

**Table S1. Molecular Sizes of Epoxides with Different Substituted Groups**

| Entry | Epoxides | Molecular model | Molecular Size (Å$^3$) |
|---|---|---|---|
| 1 | 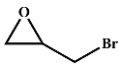 | 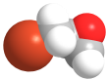 | 7.524×5.709×4.959 |
| 2 | 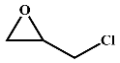 | 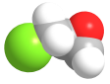 | 7.181×5.343×4.968 |
| 3 | 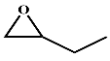 | 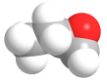 | 7.237×5.271×4.967 |
| 4 | 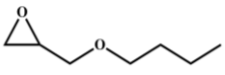 | 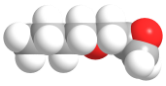 | 12.039×5.471×5.082 |
| 5 | 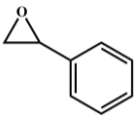 |  | 9.203×6.987×4.799 |
| 6 | 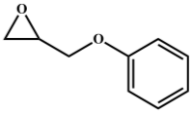 | 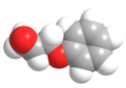 | 11.292×7.126×4.802 |

**Table S2. Comparison of Various Catalysts for Cycloaddition of $CO_2$ with Styrene Oxide**

| Compound | Catalyst (mol%) | Temp. (℃) | Pressure (bar) | Time (h) | Yield (%) | TON | TOF ($h^{-1}$) | Ref. |
|---|---|---|---|---|---|---|---|---|
| JLU-MOF117 | 0.1 | 60 | 1 | 6 | 94 | 940 | 156.7 | 2 |
| JLU-MOF116 | 0.15 | 60 | 1 | 5 | 97 | 647 | 129.4 | 2 |
| NUC-38Yb | 0.5 | 60 | 1 | 10 | 96 | 768 | 76.8 | 3 |
| Mg-MOF | 0.1 | 60 | 1 | 24 | 78 | 781 | 32.5 | 4 |
| MOF-892 | 0.32 | 80 | 1 | 16 | 82 | 256 | 16.0 | 5 |
| NUC-21 | 2 | 80 | 1 | 6 | 98 | 49 | 8.2 | 6 |
| Cat1 | 1 | 80 | 4 | 4 | 98 | 98 | 24.5 | 7 |
| NUC-53 | 0.05 | 80 | 1 | 4 | 99 | 1980 | 495 | 8 |
| NUC-45a | 0.1 | 65 | 1 | 6 | 95 | 1900 | 316 | 9 |
| Rh-PMOF-1 | 0.2 | 100 | 1 | 24 | 88 | 439 | 18.3 | 10 |
| Zn-2PDC | 0.49 | 80 | 10 | 3 | 89 | 181.5 | 60.5 | 11 |
| JLU-MOF58 (Zr) | 0.1 | 80 | 1 | 12 | 65 | 650 | 54.2 | 12 |
| **MOF-Tba** | 0.125 | 60 | 1 | 6 | 96 | 768 | 128 | This work |

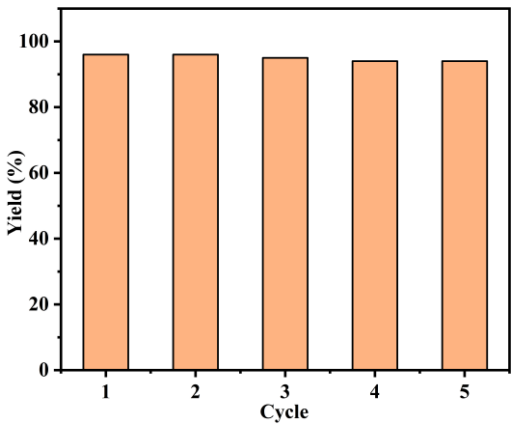


**Figure S11.** The catalytic efficiencies of **MOF-Tba** for $CO_2$ conversion within five cycles.

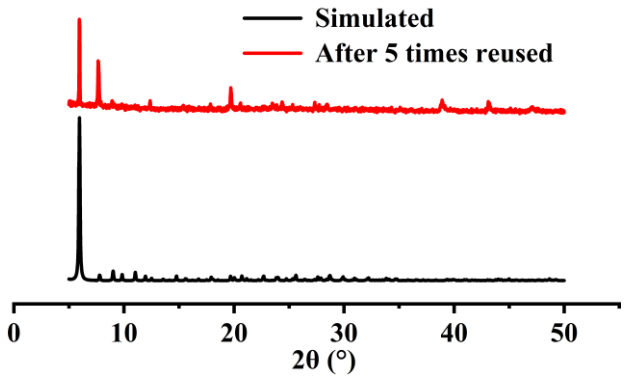


**Figure S12.** The PXRD patterns of **MOF-Tba** after five cycles of cycloadditions of styrene oxide with $CO_2$.

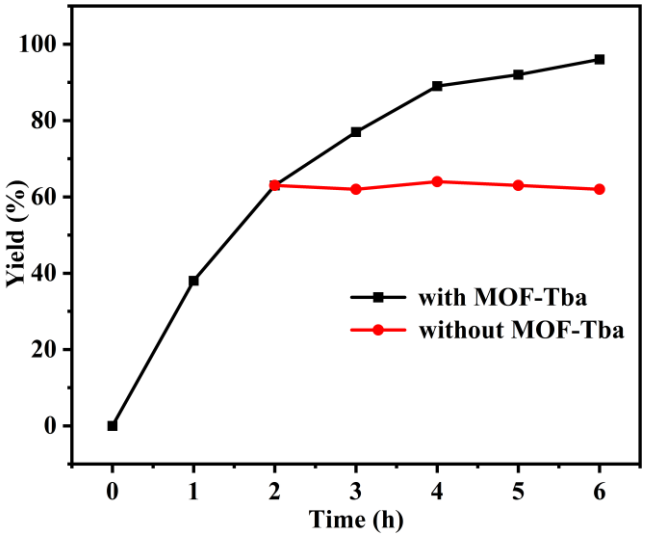


**Figure S13.** Evidence of heterogeneous nature of **MOF-Tba** in the cycloaddition reaction.

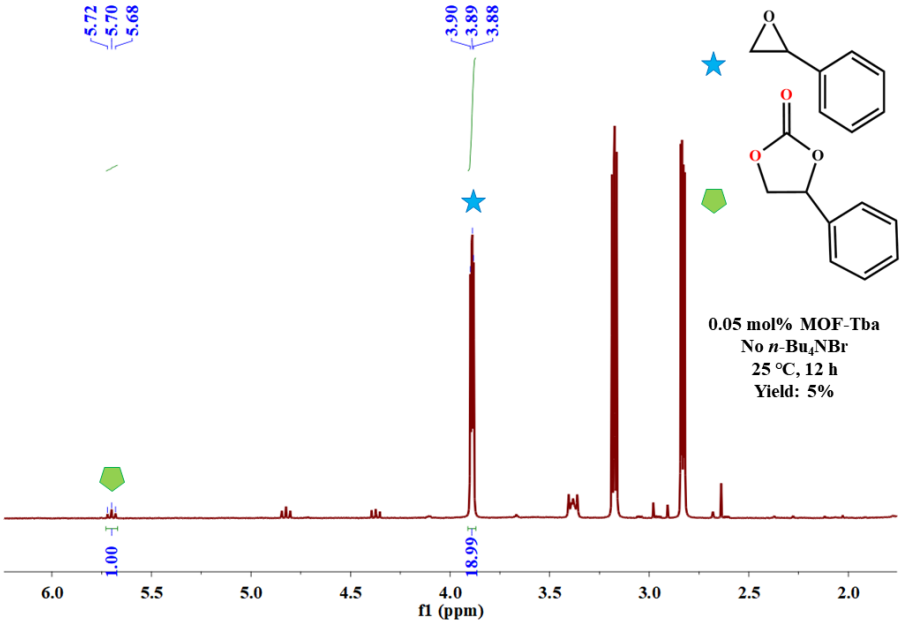


**Figure S14.** $^{1}$H NMR spectrum of $CO_2$ conversion with styrene oxide without *n*-$Bu_4NBr$ (Table 2, entry 1).

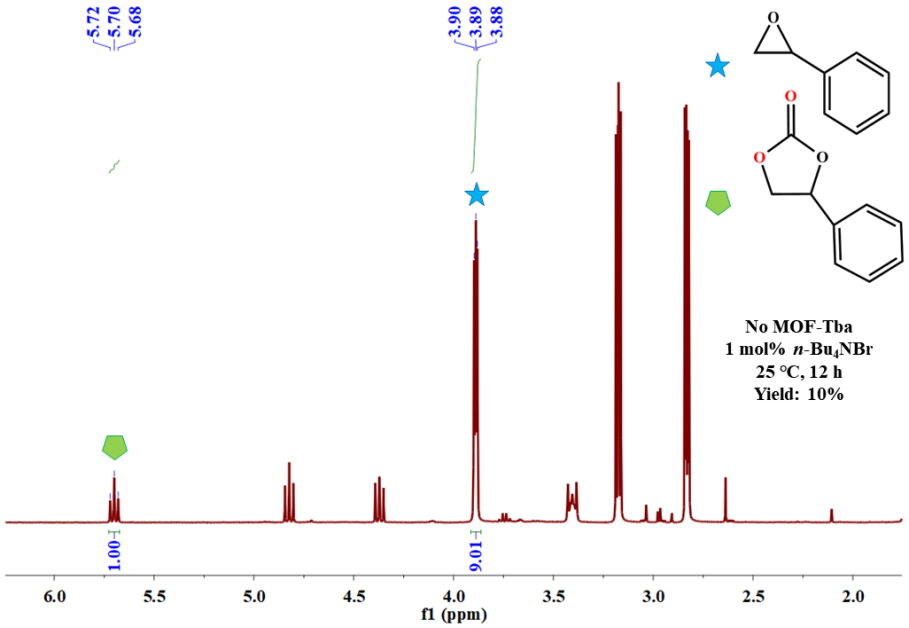


**Figure S15.** $^{1}$H NMR spectrum of $CO_2$ conversion with styrene oxide without **MOF-Tba** catalyst (Table 2, entry 2).

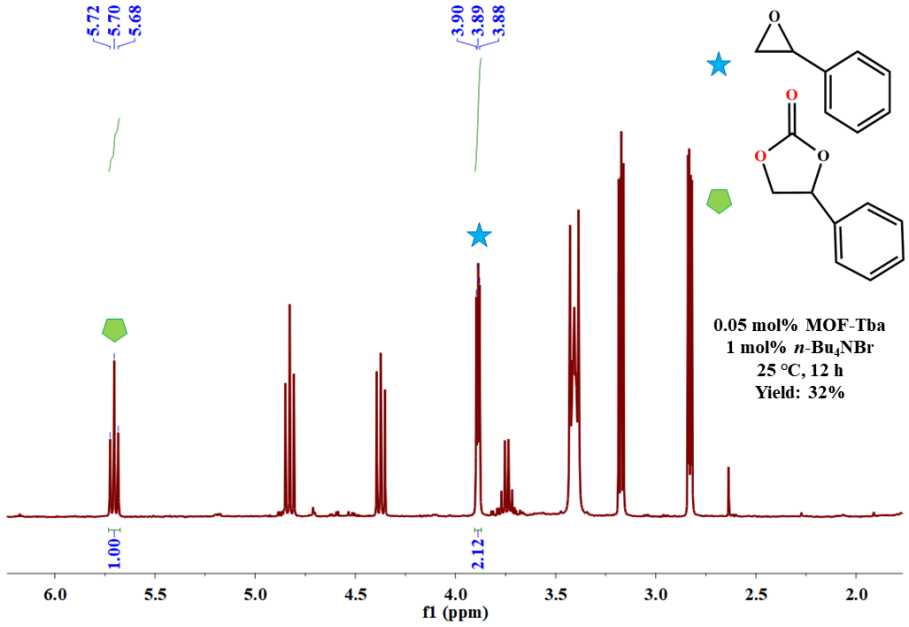


**(a)**

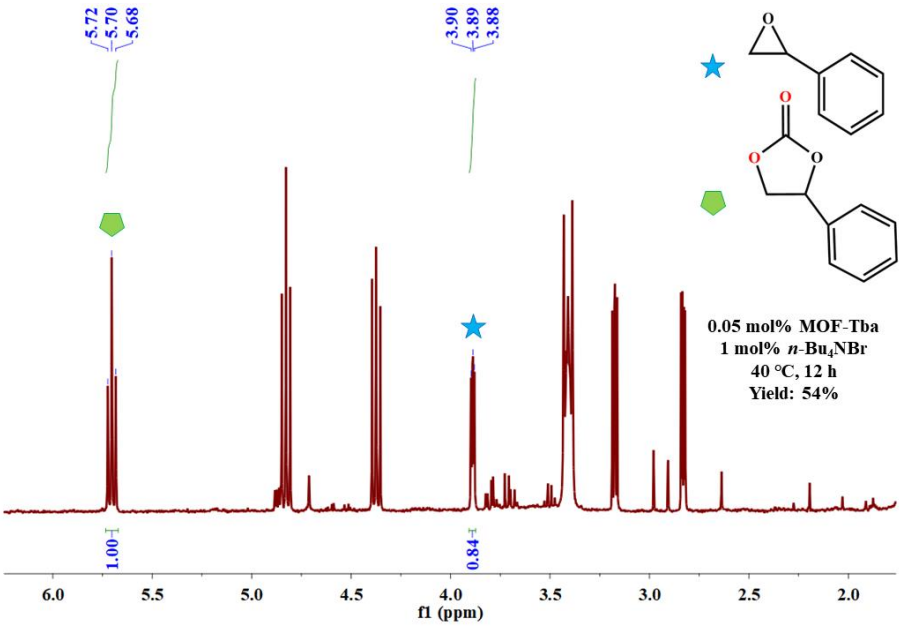


**(b)**

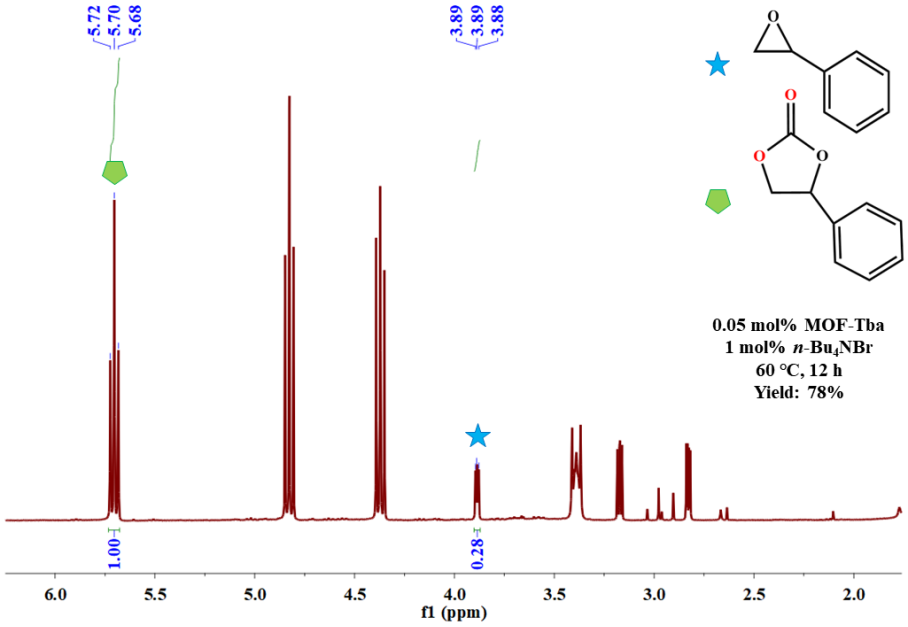


**(c)**

**Figure S16.** $^{1}$H NMR spectrum of $CO_2$ conversion catalyzed by 0.05 mol% **MOF-Tba** and 1 mol% *n*-$Bu_4NBr$ within (a) 25 ℃, (b) 40 ℃, (c) 60 ℃ (Table 2, entries 3-5).

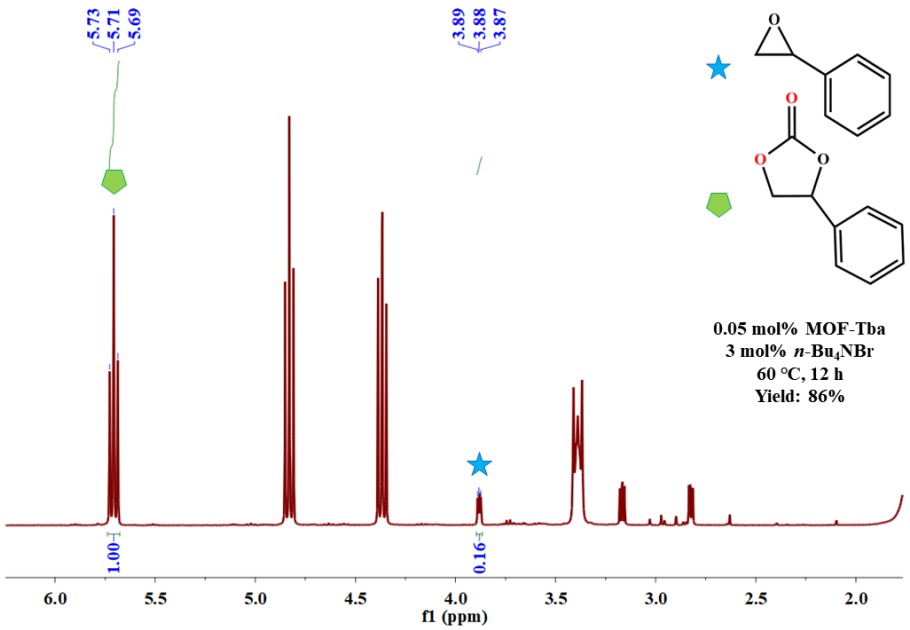


**(a)**

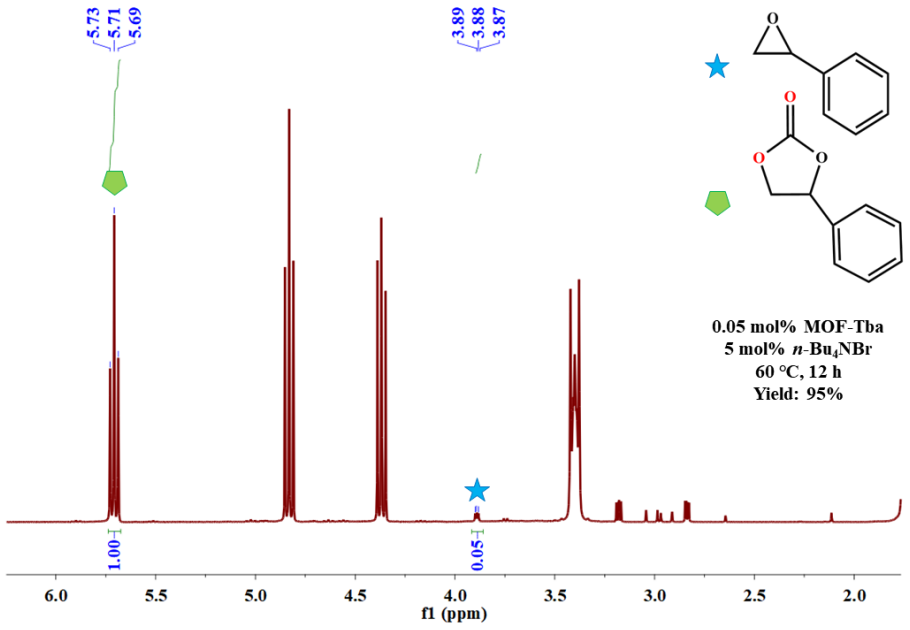


**(b)**

**Figure S17.** $^{1}$H NMR spectrum of $CO_2$ conversion catalyzed by (a) 3 mol% and (b) 5 mol% *n*-$Bu_4NBr$ and **MOF-Tba** within 60 ℃ (Table 2, entries 6,7).

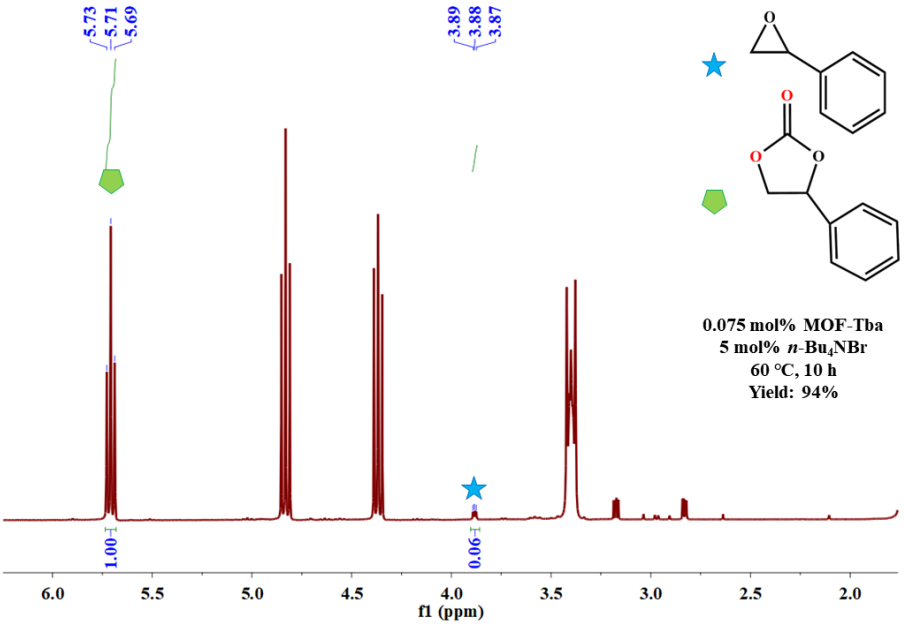
5.73
5.71
5.69
3.89
3.88
3.87
1.00
0.06
6.0
5.5
5.0
4.5
4.0
3.5
3.0
2.5
2.0
f1 (ppm)
0.075 mol% MOF-Tba
5 mol% n-Bu4NBr
60 °C, 10 h
Yield: 94%

**(a)**

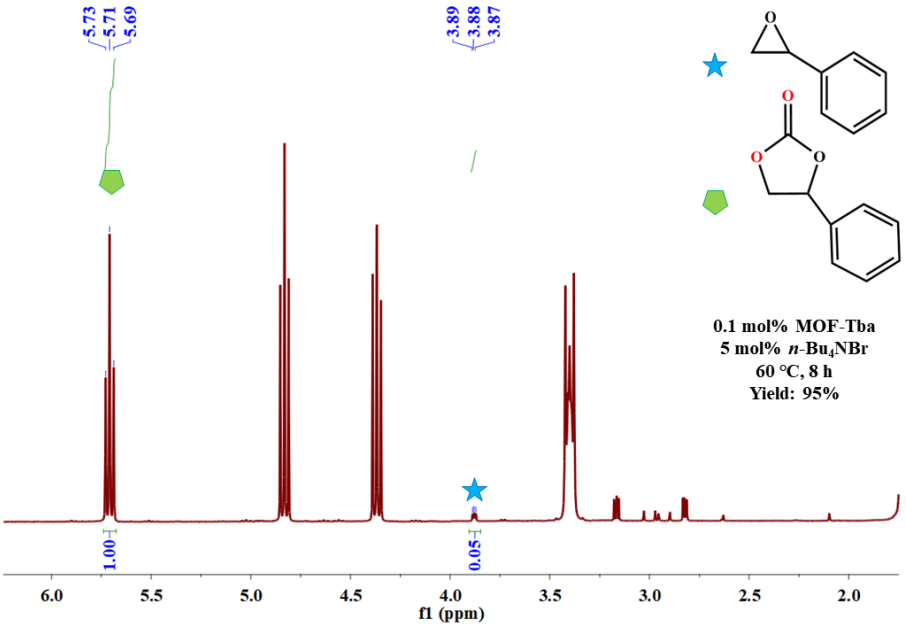
5.73
5.71
5.69
3.89
3.88
3.87
1.00
0.05
6.0
5.5
5.0
4.5
4.0
3.5
3.0
2.5
2.0
f1 (ppm)
0.1 mol% MOF-Tba
5 mol% n-Bu4NBr
60 °C, 8 h
Yield: 95%

**(b)**

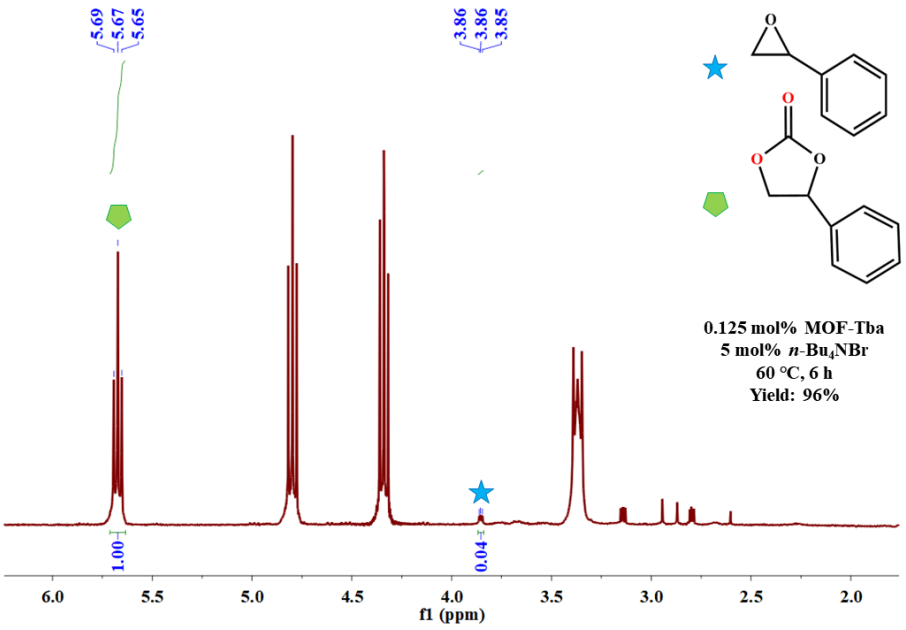


**(c)**

**Figure S18.** $^{1}$H NMR spectrum of $CO_2$ conversion catalyzed by a) 0.075 mol%, b) 0.1 mol%, and c) 0.125 mol% **MOF-Tba** and 5 mol% *n*-$Bu_4NBr$ within 60 ℃ (Table 2, entries 8-10).

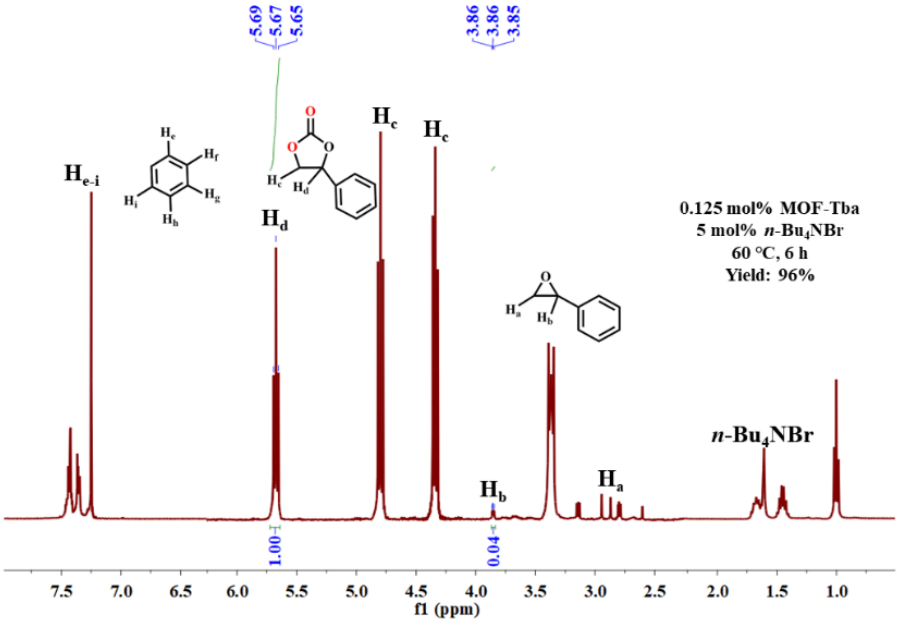


**Figure S19.** Structural analysis of $^{1}$H NMR spectrum for $CO_2$ conversion (Table 2, entry 10).

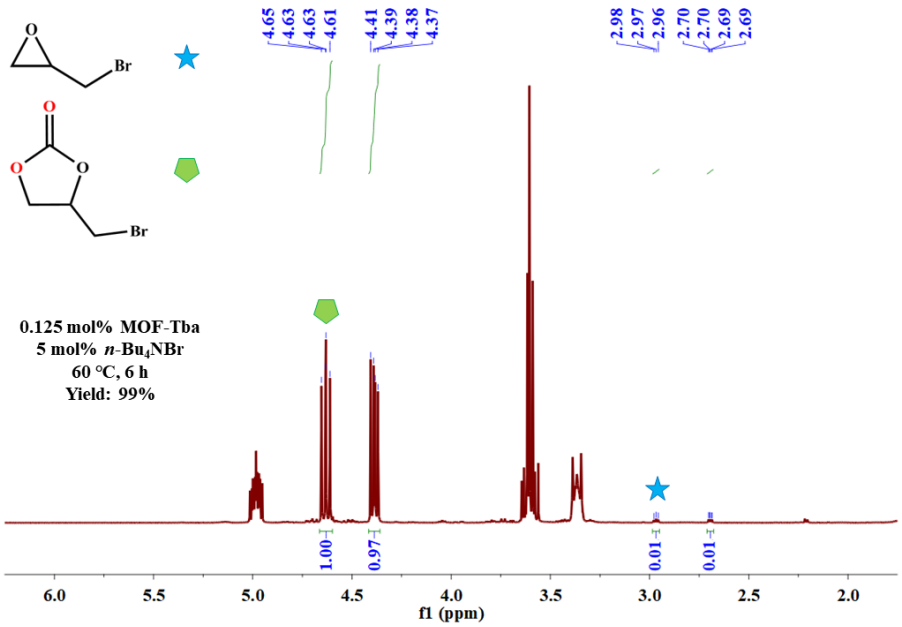


**Figure S20.** $^{1}$H NMR spectrum of $CO_2$ conversion with epibromhydrin by **MOF-Tba** (Table 3, entry 1).

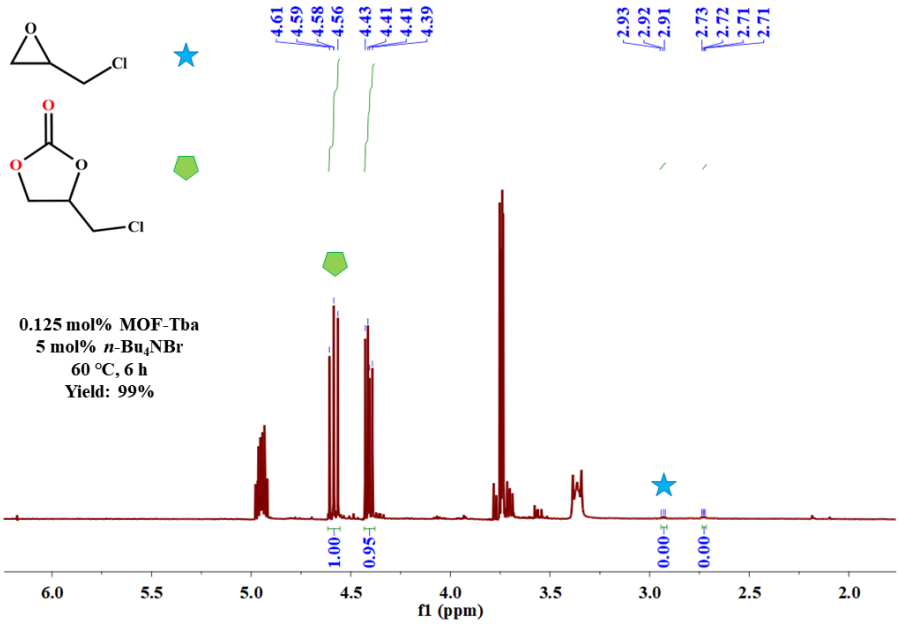


**Figure S21.** $^{1}$H NMR spectrum of $CO_2$ conversion with epichlorohydrin by **MOF-Tba** (Table 3, entry 2).

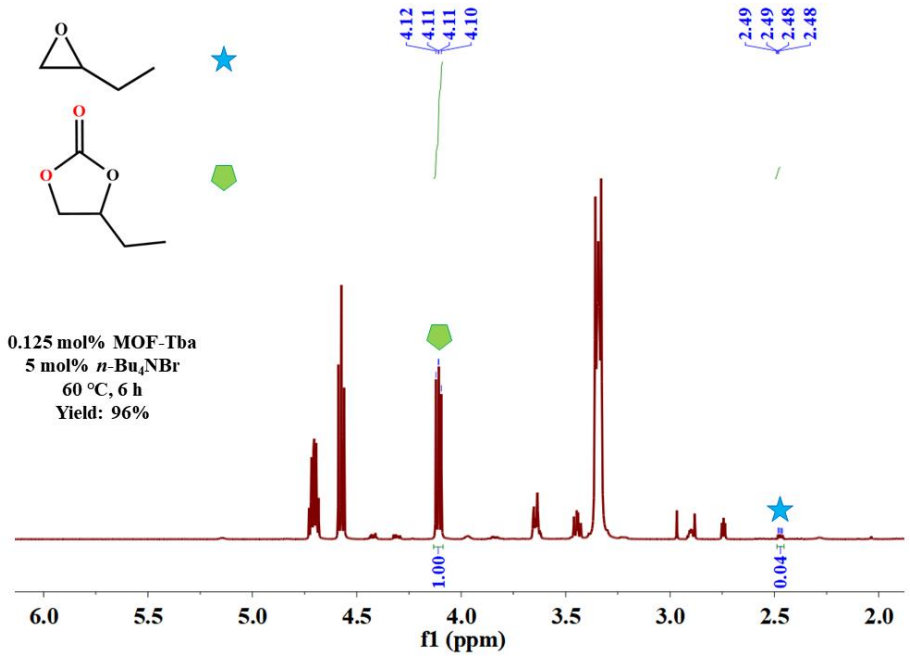


**Figure S22.** $^{1}$H NMR spectrum of $CO_2$ conversion with epoxy propane by **MOF-Tba** (Table 3, entry 3).

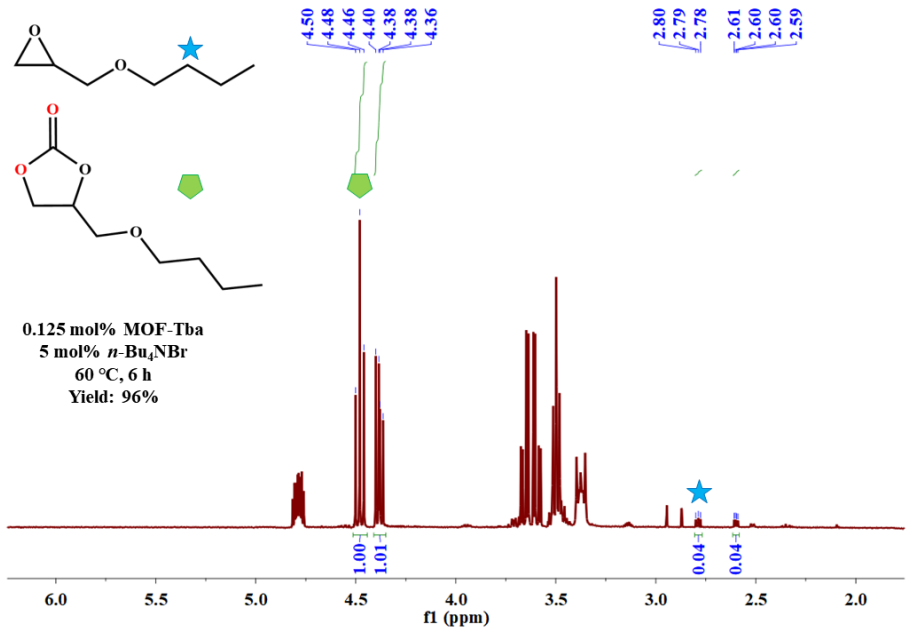


**Figure S23.** $^{1}$H NMR spectrum of $CO_2$ conversion with N-butyl glycidyl ether by **MOF-Tba** (Table 3, entry 4).

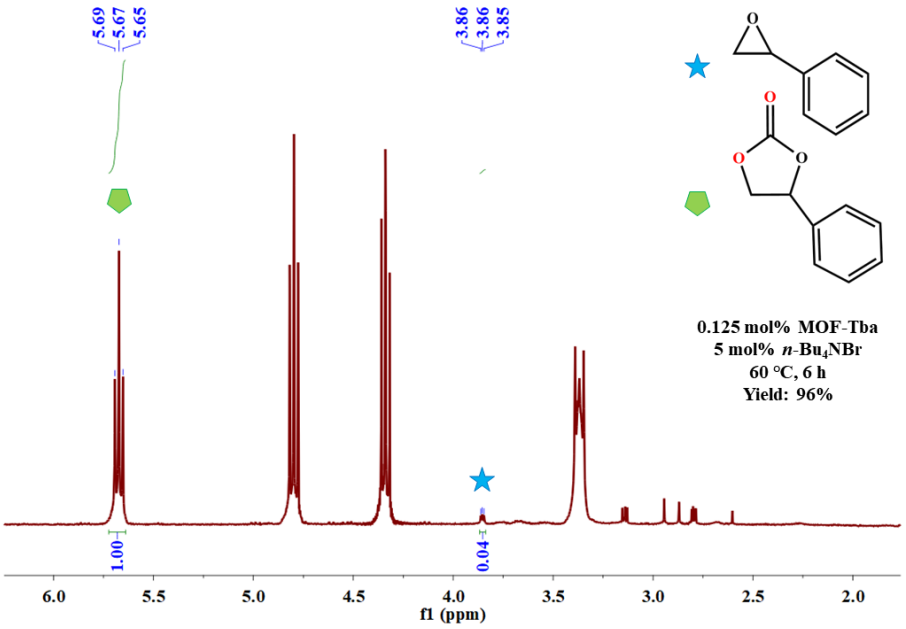


**Figure S24.** $^{1}$H NMR spectrum of $CO_2$ conversion with styrene oxide by **MOF-Tba** (Table 3, entry 5).

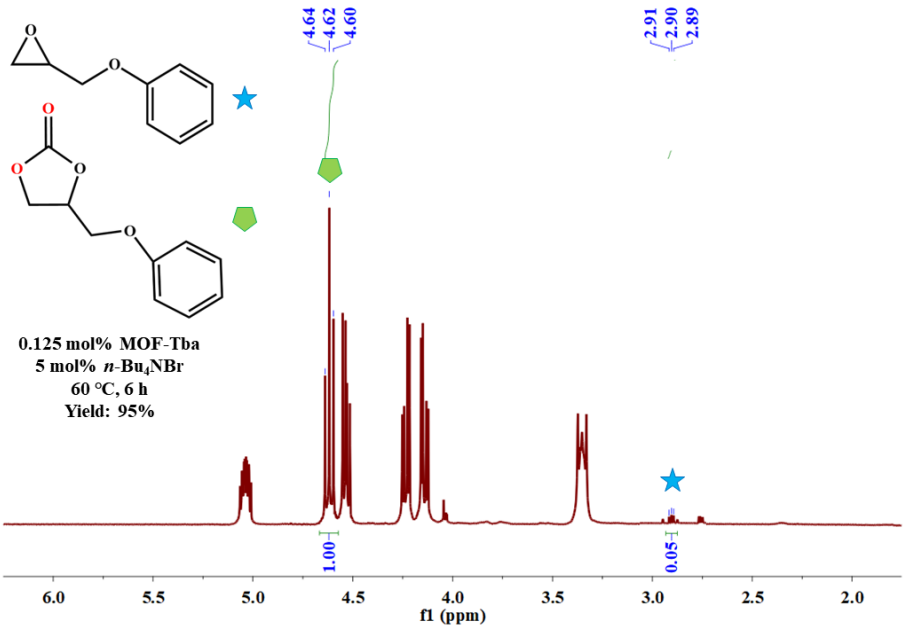


**Figure S25.** $^{1}$H NMR spectrum of $CO_2$ conversion with glycidyl phenyl ether by **MOF-Tba** (Table 3, entry 6).

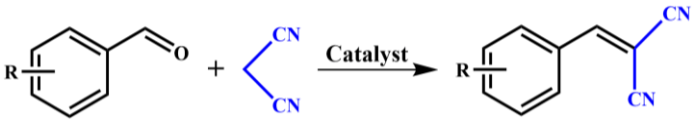


**Scheme S2.** Diagrammatic sketch of Knoevenagel Condensation reaction.

**Table S3. The Molecular Sizes of Various Benzaldehyde Derivatives**

| Entry | Substrates | Molecular model | Molecular Size (Å$^3$) |
|---|---|---|---|
| 1 | 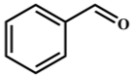 | 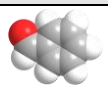 | 8.556×6.933×3.401 |
| 2 | 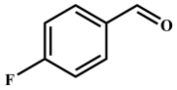 |  | 9.137×6.795×3.401 |
| 3 | 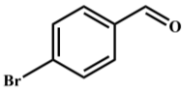 | 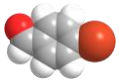 | 10.033×6.685×3.660 |
| 4 | 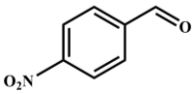 | 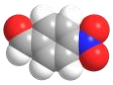 | 10.334×6.730×3.697 |
| 5 | 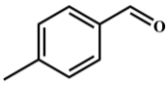 |  | 9.543×6.800×4.018 |
| 6 | 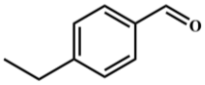 |  | 10.492×6.613×4.019 |
| 7 | 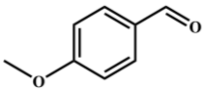 |  | 10.654×6.965×4.019 |

**Table S4. Comparison of the Catalytic Activity of Various MOFs for the Knoevenagel Condensation of Aldehyde Derivative and Malononitrile**

| Compound | Catalyst (mol%) | Solvent | Temp. (℃) | Time (h) | Yield (%) | TON | Ref. |
|---|---|---|---|---|---|---|---|
| JLU-MOF116 | 0.25 | ethanol | 40 | 2 | 95 | 380 | 2 |
| JLU-MOF117 | 0.25 | ethanol | 40 | 1.5 | 99 | 396 | 2 |
| NUC-38Yb | 0.3 | ethanol | 45 | 24 | 96 | 1280 | 3 |
| NUC-21 | 0.3 | solvent free | 70 | 1 | 97 | 323 | 6 |
| NUC-53 | 0.35 | DMSO | 70 | 6 | 99 | 283 | 8 |
| NUC-45a | 0.3 | ethanol | 50 | 12 | 99 | 660 | 9 |
| MOF3 | 0.25 | DMF | RT | 6 | 97 | 388 | 13 |
| NUC-25 | 0.4 | solvent free | 80 | 24 | 99 | 248 | 14 |
| NUC-28 | 0.3 | ethanol | 45 | 24 | 96 | 320 | 15 |
| $[Zn_2(TCA)(BIB)_{2.5}](NO_3)$ | 0.3 | ethanol | 60 | 1 | 99 | 167 | 16 |
| $[Cu_2(\mu\text{-}H_3ddba)_2(phen)_2]$ | 2 | $H_2O$ | 25 | 1 | 99 | 50 | 17 |
| **MOF-Tba** | 0.25 | solvent free | 60 | 2 | 99 | 396 | **This work** |

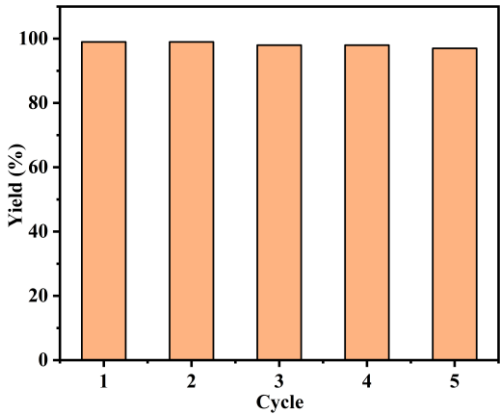


**Figure S26.** The catalytic properties of **MOF-Tba** for Knoevenagel condensation after five cycles.

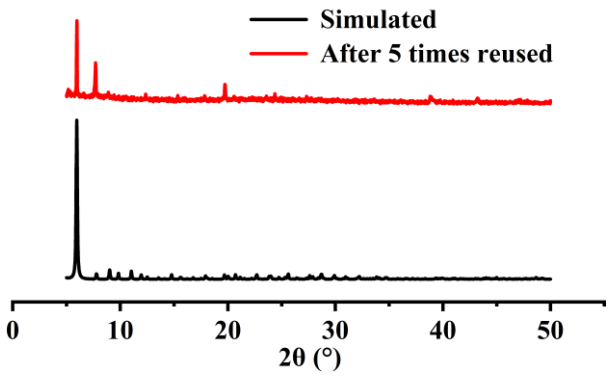


**Figure S27.** The PXRD pattern of **MOF-Tba** after recycled Knoevenagel condensation reaction.

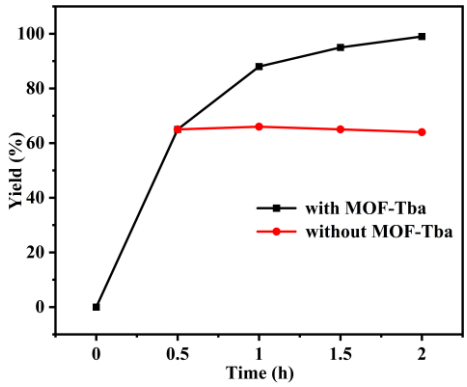


**Figure S28.** Evidence of heterogeneous nature of **MOF-Tba** in the Knoevenagel condensation.

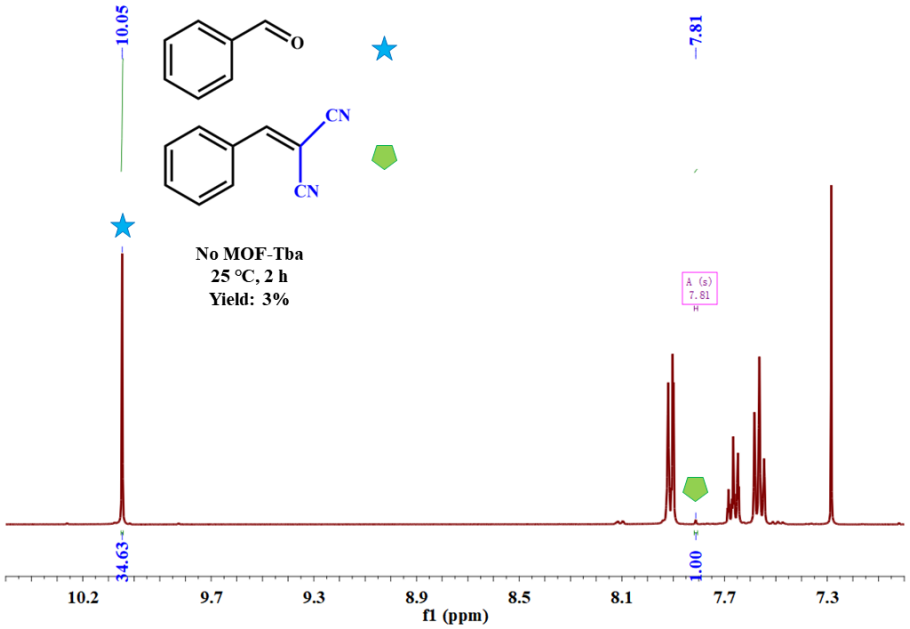


**(a)**

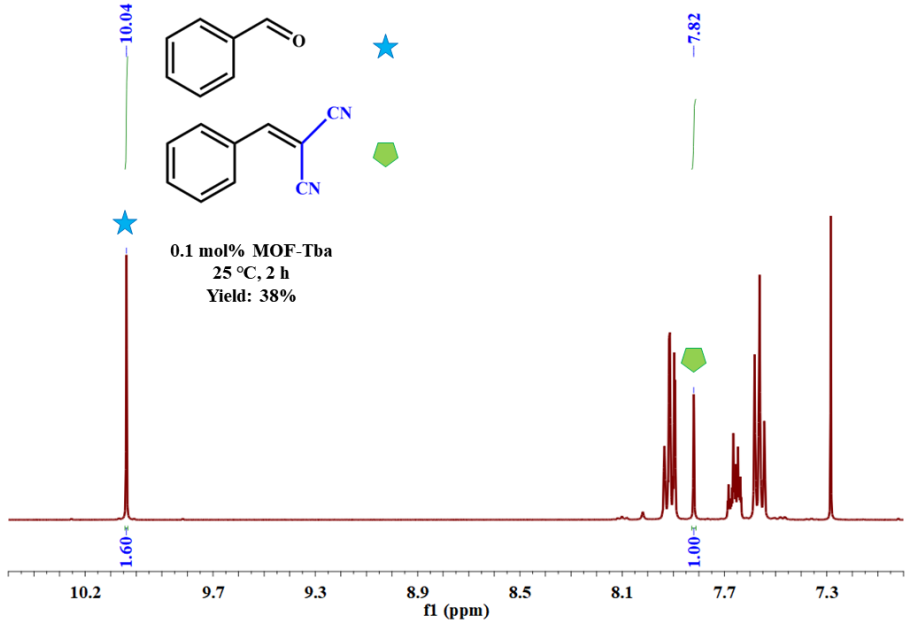


**(b)**

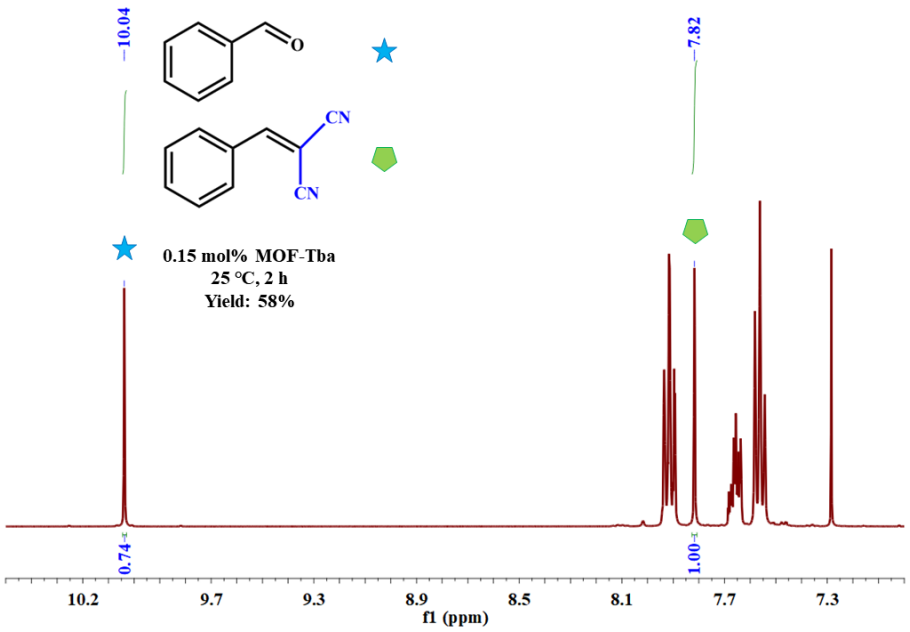
10.04
7.82
O
CN
CN
0.15 mol% MOF-Tba
25 °C, 2 h
Yield: 58%
0.74
1.00
10.2
9.7
9.3
8.9
8.5
8.1
7.7
7.3
f1 (ppm)

**(c)**

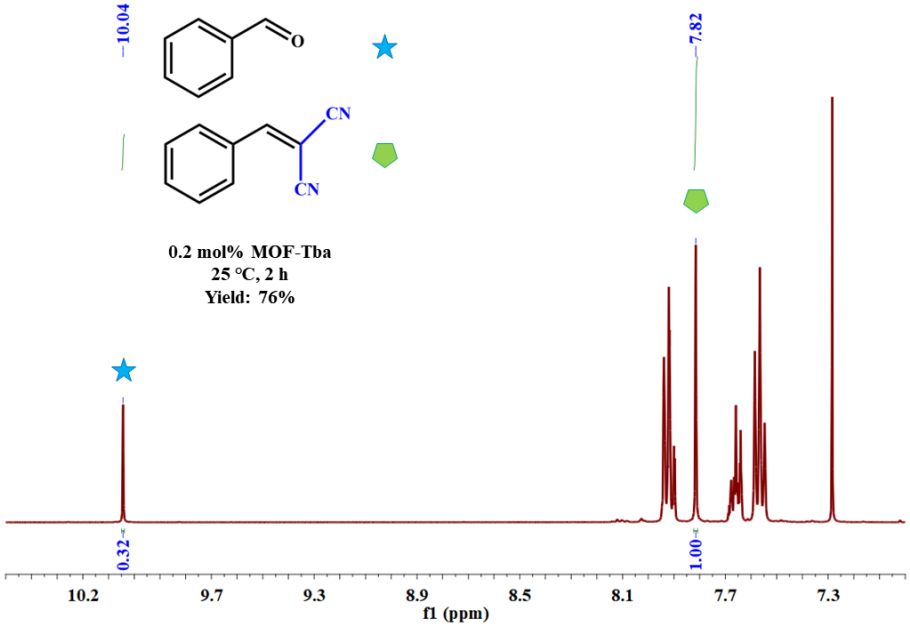
10.04
7.82
O
CN
CN
0.2 mol% MOF-Tba
25 °C, 2 h
Yield: 76%
0.32
1.00
10.2
9.7
9.3
8.9
8.5
8.1
7.7
7.3
f1 (ppm)

**(d)**

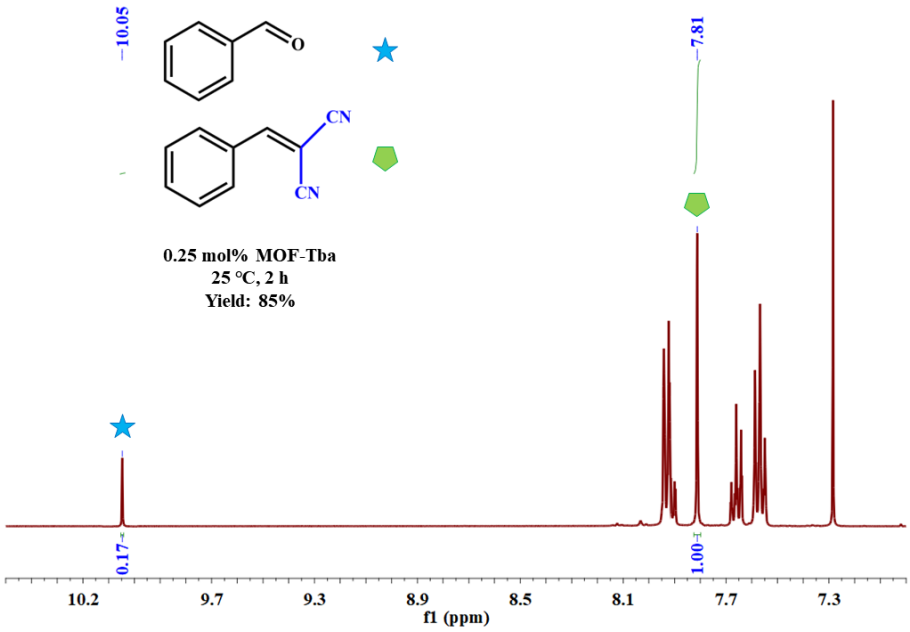


**(e)**

**Figure S29.** $^{1}$H NMR spectrum of Knoevenagel condensation reactions catalyzed by (a) 0 mol%, (b) 0.1 mol%, (c) 0.15 mol%, (d) 0.2 mol% and (e) 0.25 mol% **MOF-Tba** within 25 ℃ (Table 4, entries 1-5).

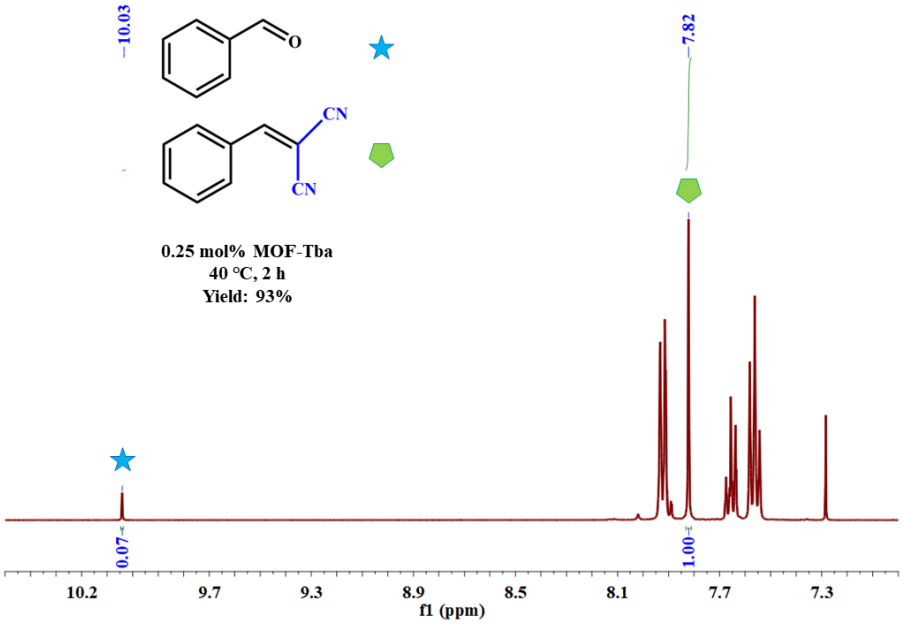


**(a)**

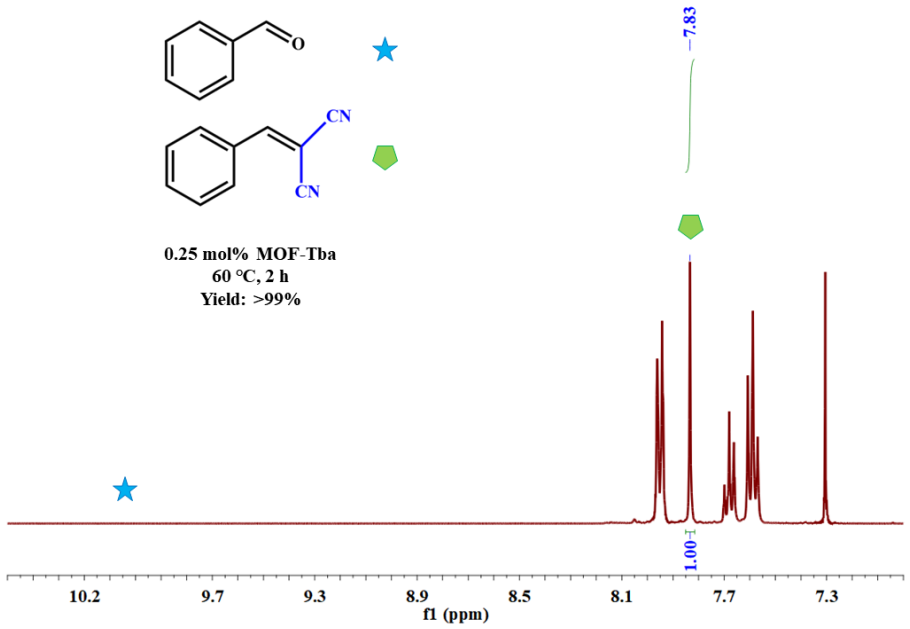


**(b)**

**Figure S30.** $^{1}$H NMR spectrum of Knoevenagel condensation reactions catalyzed by 0.25 mol% **MOF-Tba** within (a) 40 ℃ and (b) 60 ℃ (Table 4, entries 6,7).

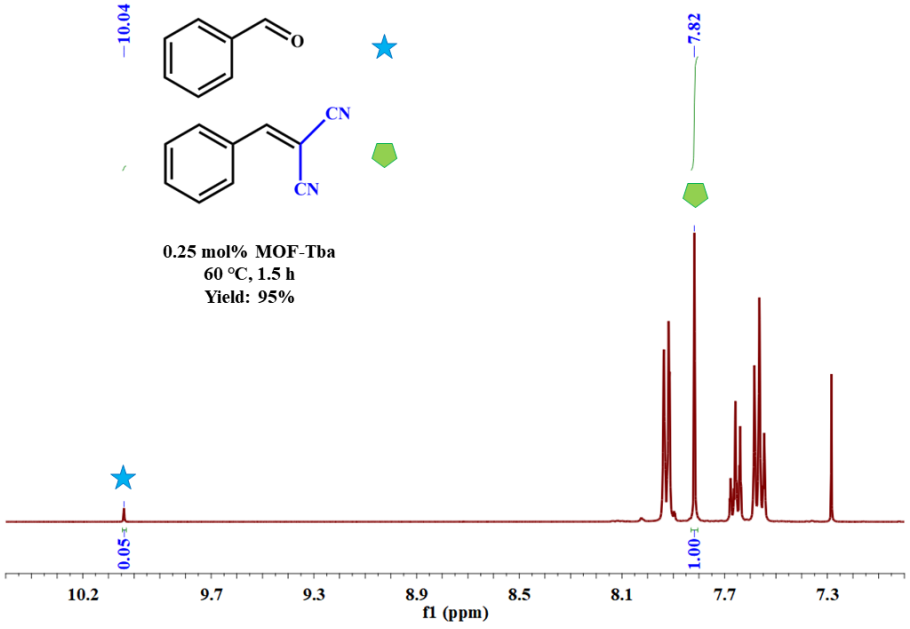


**(a)**

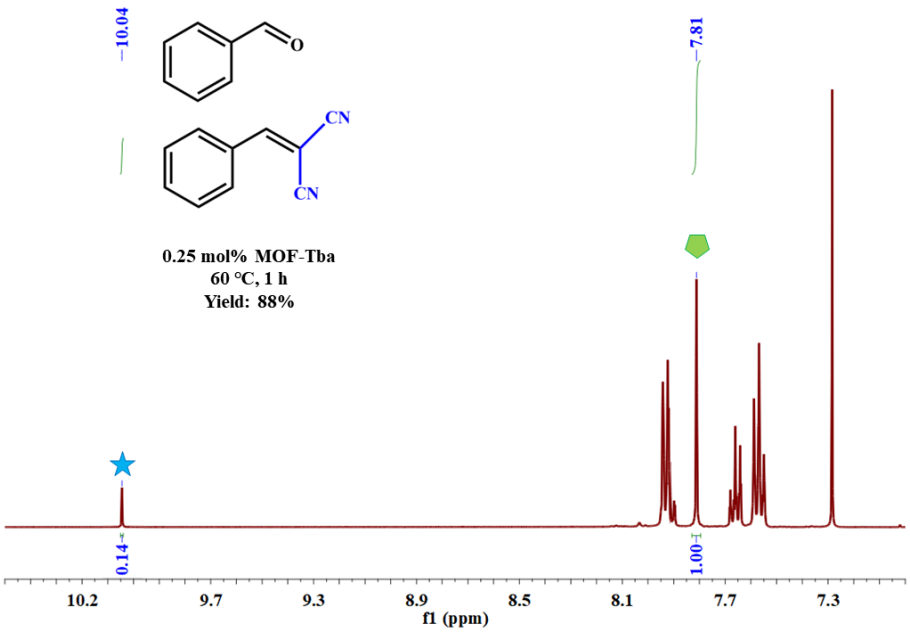


**(b)**

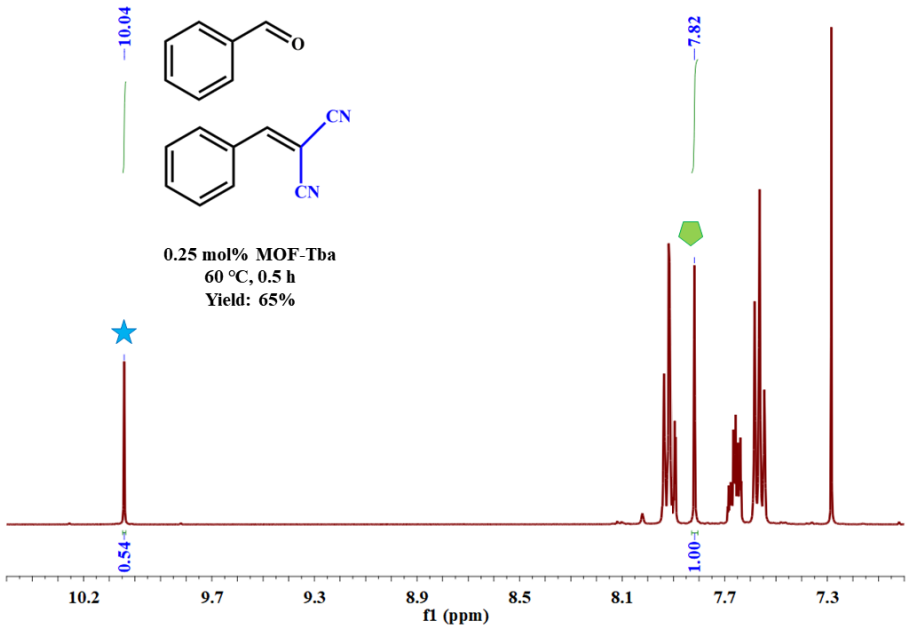


**(c)**

**Figure S31.** $^{1}$H NMR spectrum of Knoevenagel condensation reactions catalyzed by 0.25 mol% **MOF-Tba** at 60 ℃ within (a) 1.5 h, (b) 1 h and (c) 0.5 h (Table 4, entries 8-10).

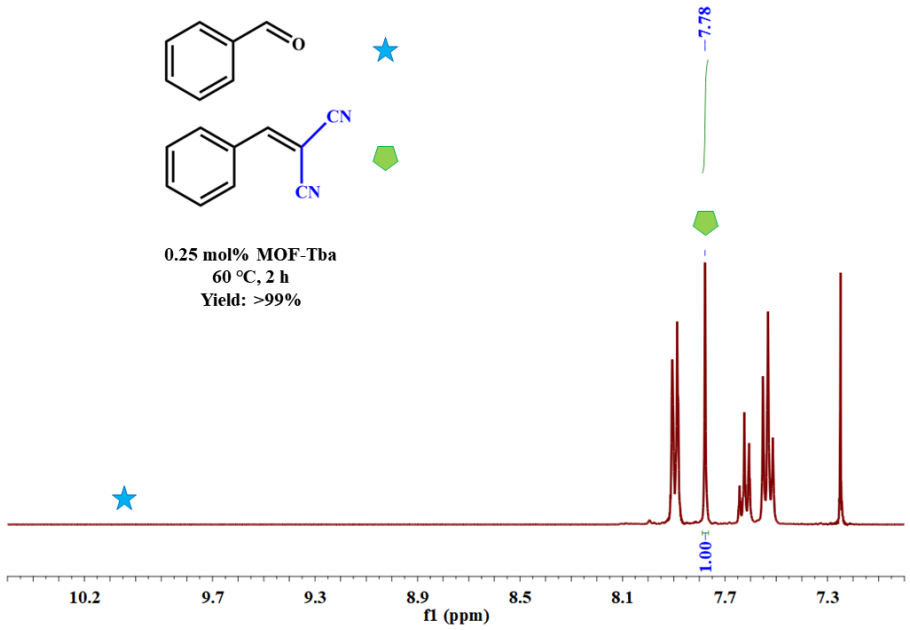


**Figure S32.** $^{1}$H NMR spectrum of the Knoevenagel condensation by **MOF-Tba** with benzaldehyde as reactants (Table 5, entry 1).

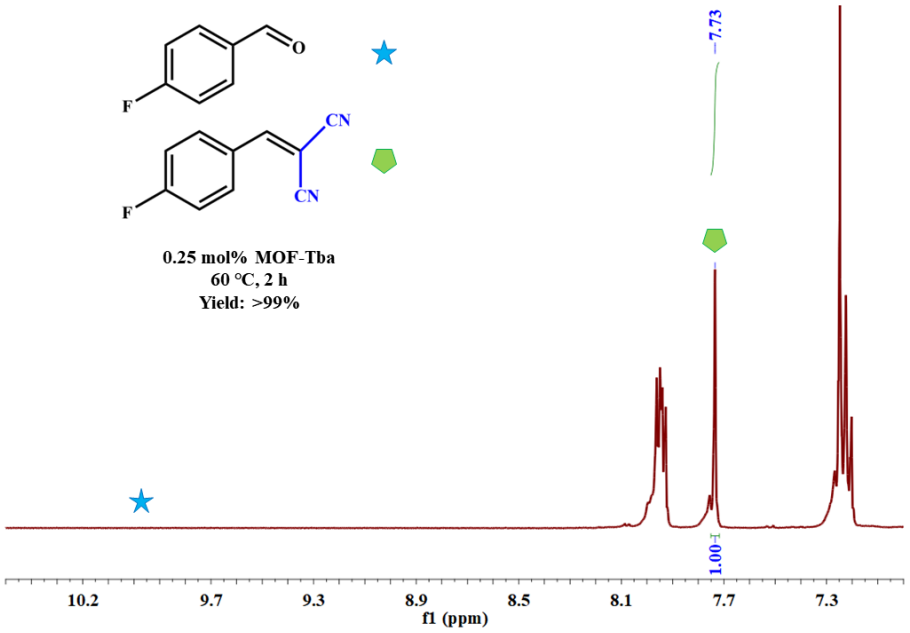


**Figure S33.** $^{1}$H NMR spectrum of the Knoevenagel condensation by **MOF-Tba** with 4-fluorobenzaldehyde as reactants (Table 5, entry 2).

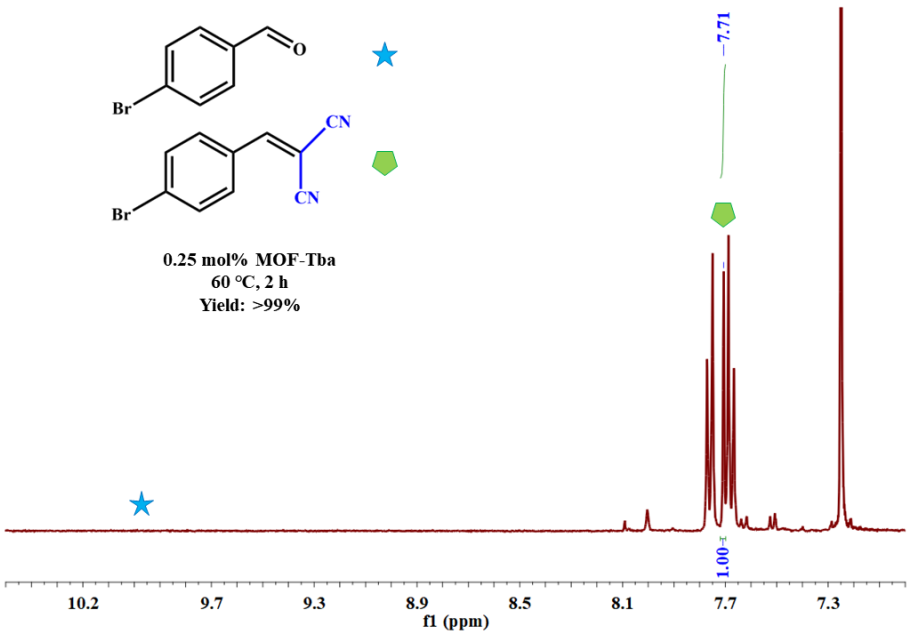


**Figure S34.** $^{1}$H NMR spectrum of the Knoevenagel condensation by **MOF-Tba** with 4-bromobenzaldehyde as reactants (Table 5, entry 3).

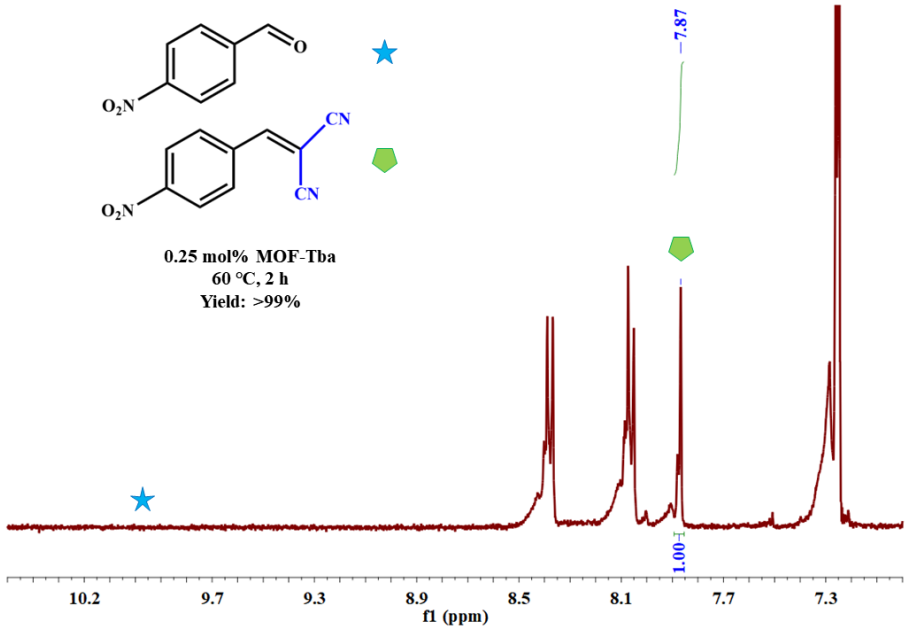


**Figure S35.** $^{1}$H NMR spectrum of the Knoevenagel condensation by **MOF-Tba** with 4-nitrobenzaldehyde as reactants (Table 5, entry 4).

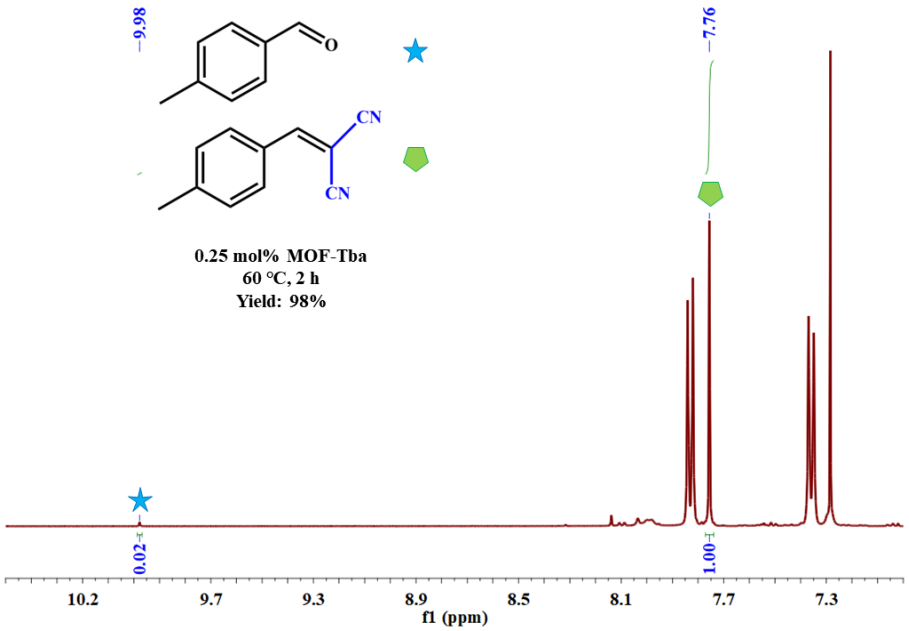


**Figure S36.** $^{1}$H NMR spectrum of the Knoevenagel condensation by **MOF-Tba** with 4-methylbenzaldehyde as reactants (Table 5, entry 5).

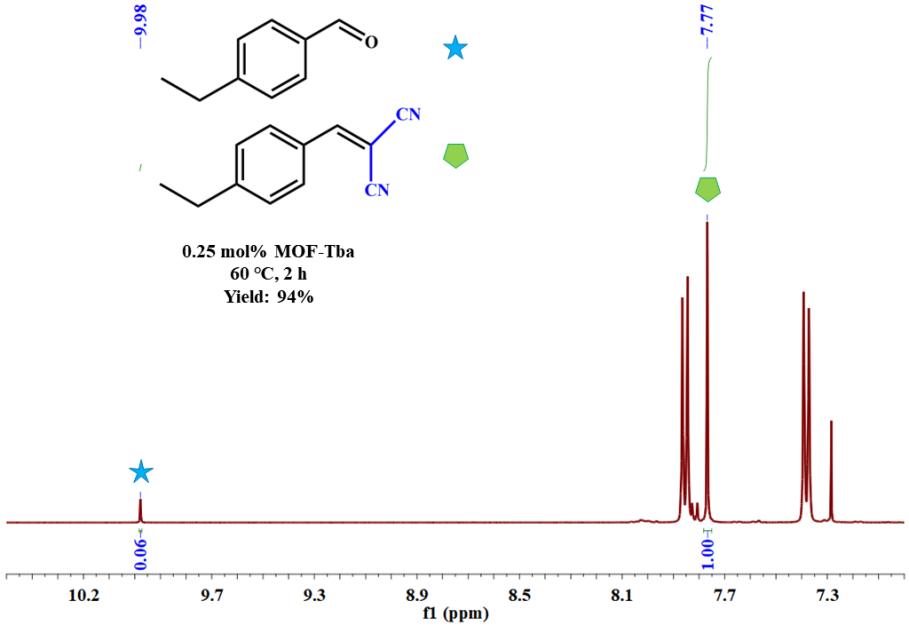


**Figure S37.** $^{1}$H NMR spectrum of the Knoevenagel condensation by **MOF-Tba** with 4-ethyl benzaldehyde as reactants (Table 5, entry 6).

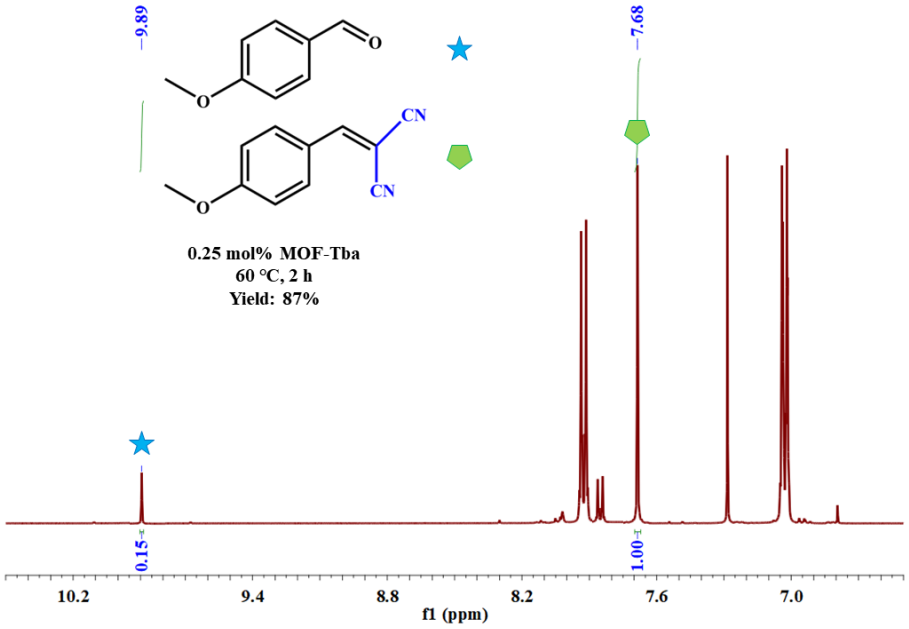


**Figure S38.** $^{1}$H NMR spectrum of the Knoevenagel condensation by **MOF-Tba** with 4-methoxybenzaldehyde as reactants (Table 5, entry 7).

## REFERENCES


1. G. M. Sheldrick, SHELXL-2014, *University of Gӧttingen, Germany*, 2014.
2. J. Qiao, B. Zhang, L. Zhang and Y. Liu, *J. Mater. Chem. A*, 2022, **10**, 17773-17781.
3. T. Zhang, H. Chen, S. Liu, H. Lv, X. Zhang and Q. Li, *ACS Catal.*, 2021, **11**, 14916-14925.
4. R. Das, T. Ezhil, A. S. Palakkal, D. Muthukumar, R. S. Pillai and C. M. Nagaraja, *J. Mater. Chem. A*, 2021, **9**, 23127-23139.
5. P. T. K. Nguyen, H. T. D. Nguyen, H. N. Nguyen, C. A. Trickett, Q. T. Ton, E. Gutierrez-Puebla, M. A. Monge, K. E. Cordova and F. Gandara, *ACS Appl. Mater. Interfaces*, 2018, **10**, 733-744.
6. H. Chen, L. Fan and X. Zhang, *ACS Appl. Mater. Interfaces*, 2020, **12**, 54884-54892.
7. M. Pander, M. Janeta and W. Bury, *ACS Appl. Mater. Interfaces*, 2021, **13**, 8344-8352.
8. H. Chen, S. Liu, H. Lv, Q. P. Qin and X. Zhang, *ACS Appl. Mater. Interfaces*, 2022, **14**, 18589-18599.
9. S. Liu, H. Chen and X. Zhang, *ACS Catal.*, 2022, **12**, 10373-10383.
10. J. Liu, Y. Z. Fan, X. Li, Y. W. Xu, L. Zhang and C. Y. Su, *ChemSusChem*, 2018, **11**, 2340-2347.
11. Y. Li, X. Zhang, J. Lan, D. Li, Z. Wang, P. Xu and J. Sun, *ACS Sustainable Chem. Eng.*, 2021, **9**, 2795-2803.
12. X. Sun, J. Gu, Y. Yuan, C. Yu, J. Li, H. Shan, G. Li and Y. Liu, *Inorg. Chem.*, 2019, **58**, 7480-7487.
13. Y. Y. Zhang, Q. Liu, L. Y. Zhang, Y. M. Bao, J. Y. Tan, N. Zhang, J. Y. Zhang and Z. J. Liu, *Dalton Trans.*, 2021, **50**, 647-659.
14. H. Chen, T. Hu, L. Fan and X. Zhang, *Inorg. Chem.*, 2021, **60**, 1028-1036.
15. T. Zhang, Z. Zhang, H. Chen, X. Zhang and Q. Li, *Cryst. Growth Des.*, 2021, **22**, 304-312.
16. A. Karmakar, A. Paul, K. T. Mahmudov, M. F. C. Guedes da Silva and A. J. L. Pombeiro, *New J. Chem.*, 2016, **40**, 1535-1546.
17. H.-R. Zhang, J.-Z. Gu, M. V. Kirillova and A. M. Kirillov, *Inorg. Chem. Front.*, 2021, **8**, 4209-4221.